

Revisiting the mass of open clusters with *Gaia* data

Anderson Almeida,¹★ Hektor Monteiro¹, Wilton S. Dias¹

¹*Instituto de Física e Química, Universidade Federal de Itajubá, Av. BPS 1303 Pinheirinho, 37500-903 Itajubá, MG, Brazil*

Accepted XXX. Received YYY; in original form ZZZ

ABSTRACT

The publication of the *Gaia* catalogue and improvements in methods to determine memberships and fundamental parameters of open clusters has led to major advances in recent years. However, important parameters such as the masses of these objects, although being studied mostly in some isolated cases, have not been addressed in large homogeneous samples based on *Gaia* data, taking into account details such as binary fractions. Consequently, relevant aspects such as the existence of mass segregation were not adequately studied. Within this context, in this work, we introduce a new method to determine individual stellar masses, including an estimation for the ones in binary systems. This method allows us to study the mass of open clusters, as well as the mass functions of the binary star populations. We validate the method and its efficiency and characterize uncertainties using a grid of synthetic clusters with predetermined parameters. We highlight the application of the method to the Pleiades cluster, showing that the results obtained agree with the current consensus in the literature as well as recent *Gaia* data. We then applied the procedure to a sample of 773 open clusters with fundamental parameters determined using *Gaia Early Data Release 3 (eDR3)* data, obtaining their masses. Subsequently, we investigated the relation between the masses and other fundamental parameters of the clusters. Among the results, we found no significant evidence that clusters in our sample lose and segregate mass with age.

Key words: Galaxy: open clusters and associations: general

1 INTRODUCTION

Open clusters are an interesting class of objects to investigate the Galaxy structure and evolution, since their distances and ages can be determined with good precision. Young open clusters can be used to investigate and understand the physics of star formation processes (see [Krumholz et al. \(2019\)](#) and [Krause et al. \(2020\)](#) for a review) and the relationship of mass to other parameters of those objects, such as distance and age, allows us to understand how they evolve dynamically over time. These properties also help to constrain the initial conditions used in N-body simulation models which investigate cluster evolution ([Pijloo et al. 2015](#); [Rossi et al. 2016](#)).

Clusters are affected and disrupted by internal processes (stellar winds, internal interactions, mass loss due to stellar evolution) and external processes (supernova, collision with molecular clouds, forces interacting with the Galactic potential) depending on their lifetime. These processes could change the mass of the clusters and reduce their size ([Spitzer 1958](#); [Joshi et al. 2016](#)) although the details are still being debated. Clusters may also dissolve with dissolution times that can depend on several factors such as initial cluster mass and internal structure, as well as on the external effects mentioned previously (see for example [Goodwin & Bastian \(2006\)](#) and [Portegies Zwart et al. \(2010\)](#) regarding massive young clusters).

The publication of data from the *Gaia* satellite has led to an increased number of open clusters for which fundamental parameters

have been determined (see [Cantat-Gaudin 2022](#), for a review). While the estimation of their mass remains challenging, various techniques have been employed using kinematic or photometric data. An important method is based on the density profile of the cluster, which is described by the King profile ([King 1962](#)). The King profile method involves fitting a King profile function to the measured density profile of the cluster, assuming that the cluster is in dynamical equilibrium. The determined core radius and tidal radius of the cluster are then used to calculate the mass. Direct use of the Virial theorem has also been used to get the cluster mass, as discussed in [McNamara & Sanders \(1983\)](#) and [Raboud \(1996\)](#). Integrated stellar luminosity function is another widely used method involving the construction of a histogram of the number of stars as a function of their luminosities and comparing it to theoretical models. Using photometric data, one of the first works to apply this strategy was [van den Bergh & Lafontaine \(1984\)](#) based on a sample of 142 clusters. In, [Piskunov et al. \(2008b\)](#) for example, the authors use the method to study the initial mass function of open clusters. However, for all strategies mentioned, lack of precise knowledge of the cluster member stars as well as their binary fractions were important sources of uncertainties.

In the pre-*Gaia* years, some results on the structure and dynamics of clusters are noteworthy due to the quality of the data and/or the method used. Below, we highlight a non-exhaustive selection of studies relevant to the present work.

Due to its proximity, Pleiades is one of the most studied open clusters, however, only in 1998 with the work of [Raboud & Mermillod \(1998a\)](#) it was possible to reliably estimate its mass based

★ E-mail: andersonalmeida_sa@outlook.com

on a list of 270 members. The authors found mass segregation in binary and individual stars with masses up to $1.0 M_{\odot}$. They estimated the mass of the Pleiades through different methods: tidal radius ($4000 \pm 4000 M_{\odot}$), Virial theorem ($720 \pm 220 M_{\odot}$), mass function integration ($950 \pm 200 M_{\odot}$) and by the sum of the stellar masses of the sample ($412 M_{\odot}$).

In [Raboud & Mermilliod \(1998b\)](#) the authors studied the radial structure of Praesepe and of the very young open cluster NGC 6231. They considered the structure and dynamics of the clusters using mass estimates of individual member stars. In both clusters, the masses of the stars were estimated only for the main sequence by means of a visual isochrone fit. The authors found mass segregation among the cluster members with a less pronounced degree of segregation in Praesepe compared to Pleiades: a surprising fact according to the authors, as ancient clusters, such as Praesepe, were expected to have a greater degree of segregation. The mass of Praesepe was estimated to be $(590) M_{\odot}$ by integrating the mass function.

Only few works present results of mass for dozens of clusters and those were mainly based on the data from 2MASS catalogue ([Skrutskie et al. 2006](#)) and stellar membership from the ground-based astrometric PPMX catalogue ([Röser et al. 2008](#)) published in MWSC ([Kharchenko et al. 2013a](#)). [Bonatto & Bica \(2005\)](#) determined the mass for 11 nearby open clusters, taking into account the unobserved main sequence stars by extrapolating the mass functions to the low mass limit of $0.08 M_{\odot}$. They also included estimates of the mass of unobserved evolved stars. They analyzed mass segregation, the dynamic evolution of clusters, and its implications for the slopes of mass functions, reporting that cluster size correlates to age, Galactocentric distance, and mass. [Piskunov et al. \(2007\)](#) and [Piskunov et al. \(2008a\)](#) derived the tidal radii and masses of 236 clusters, selected from the ASCC-2.5 catalogue, ([Kharchenko et al. 2007](#)) by fitting King profiles ([King 1962](#)). They found that the tidal radius distribution had peaked at about 1.5 pc and 7-10 pc and that most clusters have tidal masses in the range $\log(M_c/M_{\odot}) = 1.6$ and 2.8. [Bukowiecki et al. \(2012\)](#) estimated the mass of a sample of 599 clusters, converting the luminosity function into the mass function using the fitted isochrone.

[Joshi et al. \(2016\)](#) studied 1241 open clusters, with distances of up to 1.8 kpc from the Sun. Based on data from the MWSC ([Kharchenko et al. 2013b](#)) catalogue and masses from [Piskunov et al. \(2008a\)](#), the work presents statistical analyses of several fundamental parameters such as spatial position, age, size, mass, and extinction. They found that massive clusters with larger radii, within the solar orbit, tend to have better chances of surviving external interactions and that younger clusters have larger masses and tend to lose mass at rates of about $(150) M_{\odot}/\text{Myr}$.

With the availability of *Gaia* data, some works have emerged that, among other aspects, address the cluster mass estimates. For example, [Yontan et al. \(2019\)](#) studied the clusters ASCC 115, Collinder 421, NGC 6793, NGC 7031, NGC 7039, NGC 7086, Roslund 1, and Stock 21 where combining CCD UBv photometric and *Gaia* astrometric data showing that the slopes of the mass functions of the clusters are in good agreement with the value of [Salpeter \(1955\)](#). In the work of [Rangwal et al. \(2019\)](#), three clusters were analysed: NGC 6067, NGC 2506, and IC 4651. The photometric data for the clusters were converted into mass functions using theoretical models. Similar results for IC 4651 were also observed in [Pandey et al. \(1992\)](#) and [Durgapal & Pandey \(2001\)](#) where the existence of mass segregation was suggested.

Using fractal statistics, [Hetem & Gregorio-Hetem \(2019\)](#) investigated a sample of 50 young open clusters in different stages of evolution at different regions of the Galaxy. The individual stellar

masses were obtained by comparing the observed color-magnitude diagram with theoretical evolutionary tracks. The authors estimated the mass of the clusters by the sum of the individual mass of the member stars, which were determined from *Gaia DR2* astrometric data ([Gaia Collaboration et al. 2018](#)). Their results indicate that 46% of the clusters did not show mass segregation and the majority of the objects were inconclusive due to large errors, with only 4 objects showing clear mass segregation.

Combining data from *Gaia DR2*, 2MASS, WISE, APASS and Pan-STARRS1, [Bisht et al. \(2020\)](#) studied the open clusters Czernik 14, Haffner 14, Haffner 17, and King 10 and estimated their mass by integrating their mass function and concluded that all clusters are dynamically relaxed and show mass segregation.

More recently, two works have studied masses of open clusters. First, [Bhattacharya et al. \(2022\)](#), using the *Gaia eDR3* catalogue, studied 46 clusters with relatively elongated morphology to determine their tidal radii and study their disintegration. In addition, they determined the initial masses of the clusters and estimated their total observed masses using mass function integration. The authors concluded that 41 objects had some degree of mass segregation. Second, [Ebrahimi et al. \(2022\)](#) investigated 15 nearby clusters using *Gaia DR3* data. The authors use synthetic clusters, comparing their stellar populations with the observed ones to determine their current mass functions. From these mass functions, they estimate the masses and the binary fractions. They find that the obtained mass functions were consistent with a single power-law function. Also, a significant correlation between the mass function slope and the ratio of age to half-mass relaxation time was found. Their results also indicate that the less evolved objects have a mass function consistent with that of the solar neighbourhood, indicating a possible connection between the dissolution of open clusters and the formation of the Galactic disc.

In this study, we re-examine the potential correlations of open cluster masses with their ages, radius, and mass segregation, using a substantial sample of objects. We obtain updated estimates of mass using the *Gaia eDR3* catalogue ([Gaia Collaboration et al. 2021](#)) in order to investigate these relationships. In Sec. 2 we present a new procedure to obtain mass estimates of individual cluster member stars, taking into account binaries and, from those, the total cluster masses using the present-day mass functions. The section also presents an extensive validation of the results based on a set of synthetic clusters. In Sec. 3 the procedure is applied to the open cluster Pleiades, showing that the results obtained agree with others in the literature, in particular recent *Gaia DR3* mass data. In Sec. 4 we apply the method to a sample of 773 real open clusters and discuss the results, also comparing to previous literature values when available. In Sec. 5 we give our conclusions.

2 METHODOLOGY

In this study, we propose a new method to compute the masses of open clusters, here considered as the mass of member stars, which were determined through membership methods. The method is based on the determination of individual cluster member star masses using precise age, distance, metallicity, and extinction parameters obtained from *Gaia* data. To estimate the individual member star masses, synthetic clusters are generated with full control of fundamental parameters. Finally, a Monte Carlo method is used to obtain the final individual masses, as well as their uncertainties, by comparing the observed and generated synthetic clusters. From the individual masses of the stars and an estimation of the unseen mass in low mass

stars as well as remnants of evolved stars, the masses of the clusters are obtained. We validate the method by using a set of simulated observations based on synthetic clusters generated from predefined isochrones of given age, distance, extinction and metallicity as well as binary fraction.

The procedure is summarized in the steps below:

- the fundamental parameters and photometric data are obtained for a sample of open clusters from [Dias et al. \(2021\)](#), with updated values based on *Gaia eDR3* data;
- the fundamental parameters are used in the generation of synthetic clusters which will be compared to the observed one in a Monte Carlo procedure;
- the Monte Carlo procedure generates a sample of individual mass estimates for each observed cluster star;
- based on comparison to the synthetic clusters, stars are labeled as binary or not and a companion mass is estimated if appropriate;
- the final individual star masses (and companions when present) are obtained by averaging the sample of mass estimates generated by the Monte Carlo procedure;
- the binary fraction and average mass fraction of binary systems are obtained from the observed stars;
- the final uncertainties are obtained by the standard deviation of the sample of mass estimates;
- after calculating individual star masses, we obtain the present-day mass function by fitting a function to the cluster stellar mass distribution obtained via a histogram of the mass estimates;
- the fitted present-day mass function is subsequently used to extrapolate the population of unseen low-mass stars, as well as the unseen mass in remnants of evolved stars;
- the mass obtained for the observed stars (single and binary), the mass of unseen low mass stars, the mass of remnants of evolved stars and the contribution of unseen binaries are added to obtain the final mass of the cluster.

The procedure is described in more detail in the following sections.

2.1 Determination of stellar masses

In our procedure, the estimation of the mass of each member star observed in a given open cluster is the fundamental necessary step that needs to be carried out, before the cluster mass can be obtained. As mentioned previously, with the open cluster member stars defined, the Monte-Carlo method compares generated synthetic clusters to the observed ones to determine the masses of the individual member stars. To generate the synthetic cluster we need a given set of theoretical isochrones and in this work we use the Padova PARSEC version 1.2S set of isochrones described in detail in [Bressan et al. \(2012\)](#)¹. The synthetic clusters are generated with a predefined number of stars with masses drawn from a probability distribution parameterized by the well-known Chabrier initial mass function ([Chabrier 2003](#)). In this work, we adopted a number of generated stars of 10000. A fraction of binary stars of 50% is also adopted, with the binary system companion star masses drawn from a uniform distribution with values varying from 0 to the primary star mass. Photometric errors, as per the *Gaia* data definition ([Gaia Collaboration et al. 2016](#)), are also included in the synthetic cluster.

For each star in the observed cluster, we compared its magnitudes to each of the 10000 stars generated in the synthetic cluster, finding

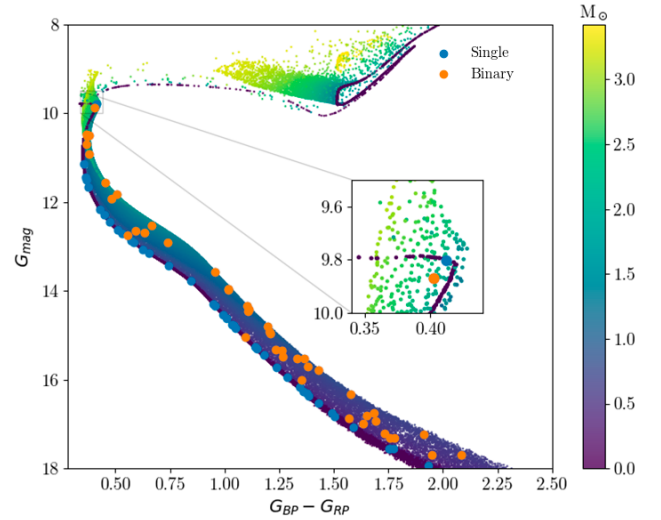


Figure 1. CMD of a simulated open cluster of $\log(\text{age}) = 8.5$, distance = 1.0 kpc and $A_V = 1.0$ mag showing 50 single and binary member stars overlaid on a synthetic cluster generated with the same referenced parameters consisting of 10000 synthetic stars. The stars in the synthetic cluster are coloured based on the mass of the companion where the main sequence is set to $M_{comp} = (0.0)M_{\odot}$. The zoom in the figure shows where the main sequence region overlaps with the binary star region.

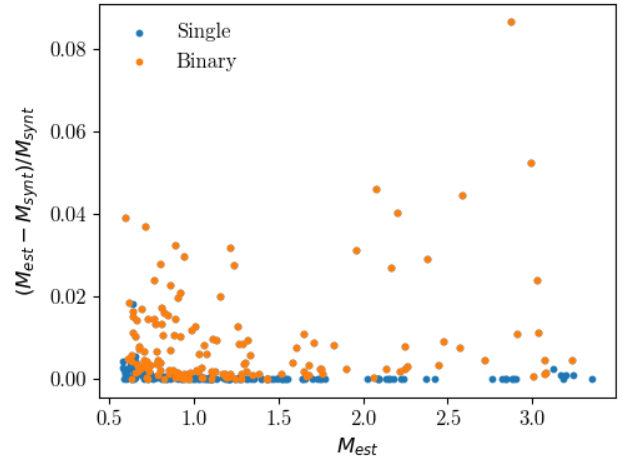


Figure 2. Test results using our mass determination method performed on a synthetic cluster of $\log(\text{age})=8.5$, distance = 1.0 kpc and $A_V = 1.0$ mag. The relative error based on the mass estimate (M_{est}) and the expected synthetic mass (M_{synt}) is presented for single stars (blue) and binary stars (orange).

the one with the smallest difference in magnitude. This step effectively finds the synthetic star with the minimum Euclidean distance from the observed one in magnitude space, according to the following equation:

$$d_i = \min_{s \in S} \sqrt{\sum_{j=1}^m (O_{ij} - S_{sj})^2}. \quad (1)$$

where d_i is the minimum distance of the star of the observed

¹ available at <http://stev.oapd.inaf.it/cgi-bin/cmd>

cluster O , to the s stars in the synthetic cluster S , measured in the j th magnitude band of the m distinct bands available (*Gaia eDR3*: G, GBP and GRP in this work).

With the closest synthetic star determined, we check if it corresponds to a binary. If it is, we mark the observed star as a binary and assign to it the corresponding primary and secondary masses, since for the synthetic cluster those are known. Else, we assign the mass of the nearest synthetic cluster star to the observed star. The process is repeated a large number of times, each time with a distinct synthetic cluster generated by varying individual stars. The final mass of the observed stars and their companions are adopted as the median of the respective sample of masses determined. The errors are obtained by the standard deviation of the estimates in each case. We note here that, since the method determines masses based on the minimization of Euclidean distances in magnitude space, the distribution of binary system companion masses is adopted for the synthetic cluster solely to efficiently sample the CMD region where binaries are likely to be located. The actual distribution of mass fractions in binary systems for a given observed cluster is determined a posteriori from the estimated stellar masses. The procedure is illustrated in Fig. 1 where we have generated a simulated open cluster with 50 member stars overlaid on a synthetic cluster generated with the same referenced parameters with 10000 synthetic stars.

To validate the stellar mass estimation method, a grid of synthetic clusters was generated with $\log(\text{age})$ varying from 6.6 to 9.5; reddening from 0.5 to 3.0 magnitudes; distances from 1 to 5 kpc and with 300 observed stars, 50% of which are binary systems. We then compared the results of our mass estimation procedure to the input masses of the generated grid. In Fig. 2 we show an example of the validation for a simulated cluster of $\log(\text{age}) = 8.5$, distance = 1.0 kpc, and $A_V = 1.0$ mag. We can see that results are in good agreement with the input synthetic masses, with binary systems showing larger differences as expected.

The individual mass estimates also vary with respect to cluster ages and distances, as shown in Fig. 3. As expected, the relative errors are worst for binaries and increase with age and distance, also with increasing spread. The behaviour is expected as the photometric errors affect proportionally more the clusters at higher distances. Young clusters also show larger uncertainties due to their more undefined turn-off region in colour-magnitude space.

We tested the efficiency of the binary detection feature in relation to other parameters of the simulated clusters and found some relevant systematic effects as a function of distance and of extinction A_V . In Fig. 4 we show the result of comparing the fraction of binaries found by the mass estimation method to the known binary fraction, adopted as 50% for the whole grid of simulated clusters. We can see a clear overestimation of the binary fraction with the increase of both distance and extinction, as well as age. For clusters with $\log(\text{age}) < 9.0$ and distance smaller than about 2.5 Kpc, the overestimation is about 20%. This effect is a result mainly of the increased uncertainty in the fainter magnitudes and the smaller sampling of the main sequence region for clusters at higher ages and distances.

Despite the good accuracy and precision shown in our method, we should note some limitations. In particular, detecting binary stars is a problem in regions of the CMD where the main sequence and binary star regions overlap. In Fig. 1 we present a plot of a CMD of a simulated open cluster of $\log(\text{age}) = 8.5$, distance = 1.0 kpc and $A_V = 1.0$ mag showing 50 single and binary member stars overlaid on a synthetic cluster generated with the same referenced parameters consisting of 10000 synthetic stars. Parallel to the main sequence, the region of binary stars can be seen as well as the effect of the varying companion masses, such as the horizontal sequence at about $G \sim 9$.

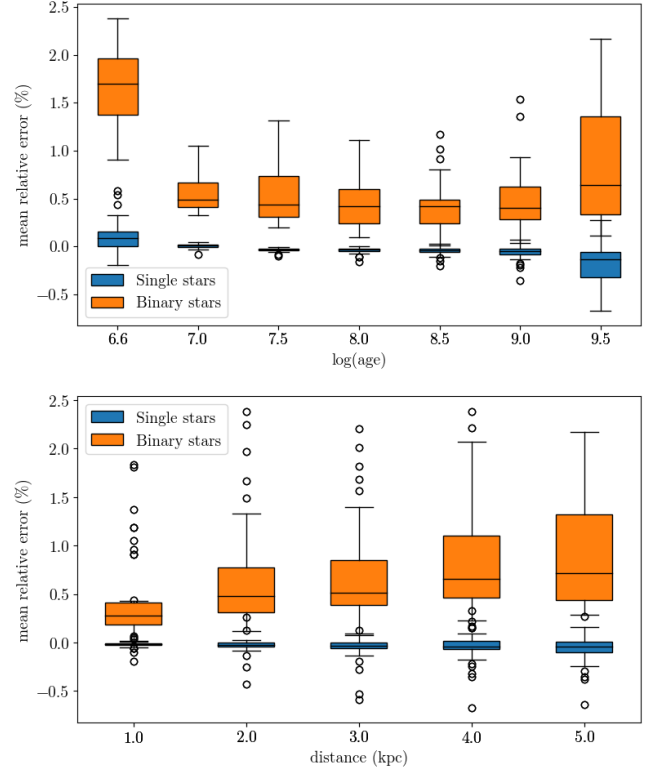


Figure 3. Mean relative error committed in the estimate of individual stellar masses as a function of the cluster age and distance.

The zoom in the figure shows the main sequence region where an overlap with the binary star region occurs at about $G \sim 10$. It is very difficult to define a constraint to determine a correct mass value in these regions of the CMD. Fortunately, this problem occurs in small regions only. Also, in most cases, the mass estimation error is usually small and does not show systematic trends, as can be seen in Fig. 2.

2.2 Determination of cluster masses

With the individual masses of the member stars of a given observed cluster, we can obtain its mass by considering the observed mass and an estimation of the unobserved mass. To estimate the unobserved mass in low mass stars, we obtain the present-day mass function from the observed star masses and extrapolate it to the lower mass limit of $0.09M_{\odot}$, adopted based on the limit of the isochrones used. We also estimate the unobserved mass of evolved stars by extrapolating in the high mass interval, if necessary, and obtaining the number of stars that have evolved to white dwarfs. In our work, we assume that the mass function can be represented by a two-part segmented linear function, which is then fit to the mass distribution of observed stars and extrapolated to the lower mass limit. The two-part segmented linear function is defined as:

$$f(x) = \begin{cases} \alpha_B x + b_1, & \text{if } x \leq M_c \\ \alpha_A x + b_2, & \text{if } x > M_c \end{cases} \quad (2)$$

where α_A and α_B represent the slopes of the function for the high mass slope and low mass slope, and b_1 and b_2 are the corresponding intercepts, respectively. M_c is the mass value at which the transition

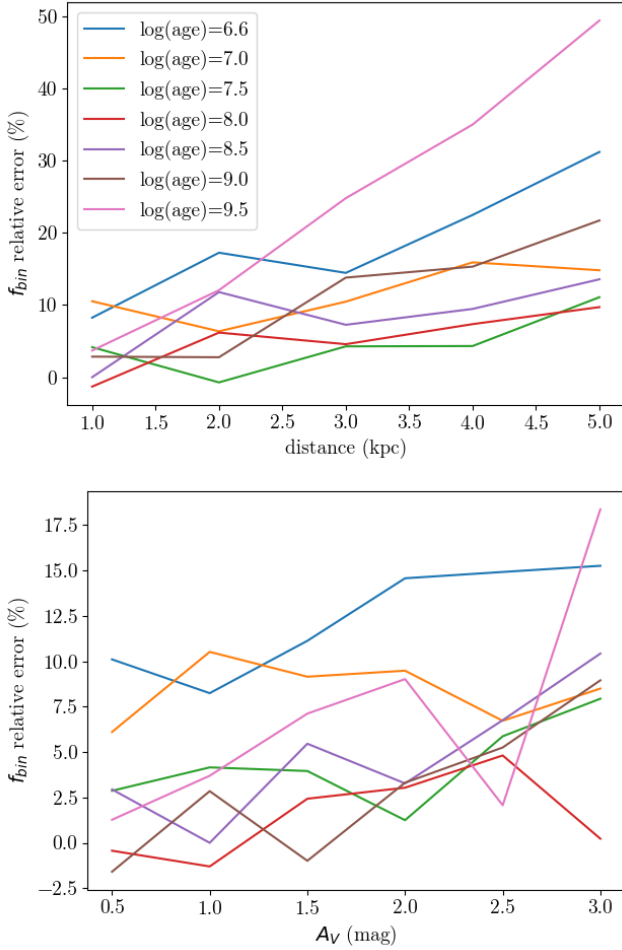


Figure 4. Relative error of the binary fraction (f_{bin}) found by the mass estimation procedure considering the known fraction (adopted as 50% of binaries) in simulated clusters. In the upper panel where the dependence to distance is investigated, we set $A_V = 1.0$ and in the lower panel where the dependence to A_V is investigated we set distance to 1kpc.

between the two linear segments occurs. In our fitting procedure α_A , α_B and M_c are free parameters and b_1 and b_2 are taken such that $f(M_c^-) = f(M_c^+)$.

The segmented linear function is fitted to a histogram for the mass distribution, where the number of bins is obtained using the rule of [Sturges \(1926\)](#). The fits were performed using the routine `curve_fit`² with the default Trust Region Reflective algorithm. The fits were done for the entire original sample³ of 1743 open clusters from [Dias et al. \(2021\)](#). We then evaluated each result to select only those that satisfied the requirement that the histogram for the mass distribution had at least 2 bins on both sides of the fitted transition mass point M_c . The final cluster sample consists of 773 objects that satisfied this criterion.

The unobserved mass of evolved stars is obtained by estimating

how many of the cluster stars have evolved to white dwarfs, which are typically not detected due to their low luminosity. To achieve this, we use the initial to final mass relation for progenitor stars from 0.85 to $7.50M_\odot$ provided by [Cummings et al. \(2018\)](#). From the fitted mass function, we calculate the number of stars in that mass range and then use the relation to obtain the present-day mass in white dwarfs.

The unobserved mass in the low mass range is obtained by integrating the mass function from the lowest observed mass to the low mass limit of $0.09M_\odot$. The unobserved low mass range is defined by low luminosity stars not detected by *Gaia*, or stars with magnitudes greater than 19, which were removed from our sample due to *Gaia*'s incompleteness limit. This procedure is similar to the one adopted by [Bonatto & Bica \(2005\)](#).

It is important to note that in this step, we do not include the masses of the binary companion to construct the present-day mass function. Since we do not know the distribution of binaries in the unobserved portion, we estimate their contribution to the mass by first obtaining a mean mass fraction for binary systems, given by $q = M_{secondary}/M_{primary}$, from the observed stars. We then obtain the binary system mass from the estimate of primary masses in the unobserved mass interval. For these systems, we assume that the primaries are distributed according to the mass function determined by the observed stars. The total unseen mass of primaries is estimated by integrating the extrapolated observed mass function down to the lower mass limit. The contribution of secondaries is found by multiplying this value by the estimated mean mass fraction to obtain the masses of the companions, thus giving the final mass in binaries. The unobserved mass will be a sum of the mass of single stars and binary systems down to the lower mass limit. The binary fraction used is also determined from the observed stars. The final mass of the cluster is then estimated by:

$$M_T = M_o + M_{un}(1 + F_{bin} \times q) + M_{WD} \quad (3)$$

where M_T is the mass of the cluster, M_o is the mass estimated from observed stars, M_{un} is the mass obtained from the integrated mass function for unobserved stars, F_{bin} and q are the estimated fraction of binaries and mean mass ratio in binary systems respectively, estimated from the observed stars and M_{WD} is the estimated mass of white dwarfs.

To exemplify the extrapolation of the unobserved region of low-mass stars, in [Fig. 5](#) we show a mass function obtained for a simulated open cluster with 600 stars with $\log(\text{age})=8.5$, at a distance of 500pc, $A_V=1.0$, $[\text{Fe}/\text{H}]=0.0$, the mass of $1043M_\odot$. The segmented line fit (green line) to the simulated observation (orange dots) is also shown. We see from the figure that the segmented line function fits well to the higher mass end of the mass function while less to the lower mass section, especially the unobserved low mass region (blue dots) which is generated from a [Chabrier \(Chabrier 2003\)](#) initial mass function. The mass obtained with the fit to the integrated mass function in this example was $1071M_\odot$, in agreement with the mass of $1043M_\odot$ of the simulated cluster.

The *Gaia eDR3* data quality has improved significantly the definition of open cluster members and features in the CMDs, enabling the determination of mass functions for individual, primary, and secondary stars in some cases. Consequently, we were able to investigate two methods to calculate the masses for a subsample of the open clusters:

- **mass function:** the determination of the mass of a cluster as described previously, where we obtain a mass function with all the observed stars, excluding binary companions, and from that, estimate the unseen mass including the contribution of binaries;

² https://docs.scipy.org/doc/scipy/reference/generated/scipy.optimize.curve_fit.html

³ A sample of the sequence including the functions used is available at https://github.com/ander-son-almeida/DashboardOCmass/blob/main/examples/MF_example.ipynb

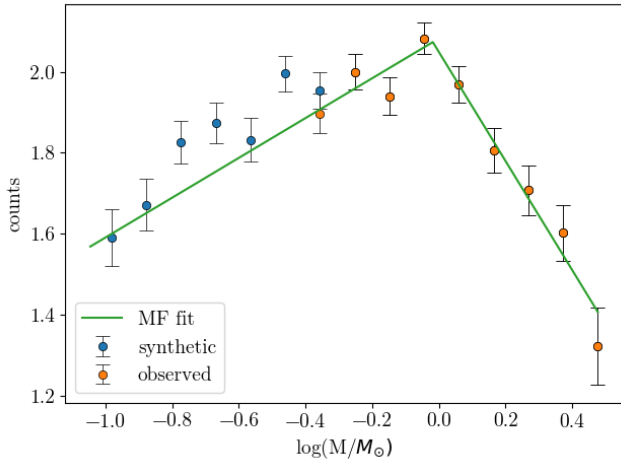


Figure 5. Synthetic open cluster of $\log(\text{age}) = 8.5$, distance = 0.5 kpc, $A_V = 1.0$ mag, $[\text{Fe}/\text{H}] = 0.0$, the mass of $1043M_\odot$ and the respective segmented line fit to the simulated observation (orange dots). The estimated unseen mass is the region defined by the blue dots, where the fitted function is used to obtain the integrated mass.

- **detailed mass function:** the determination of the mass of the cluster by summing the observed star masses to the contribution of unobserved stars as determined from mass functions determined for single, primary and secondary stars separately.

To validate both procedures and to investigate their limitations, we again make use of the grid of synthetic clusters with different parameters. In Fig. 6 we present the distribution of the relative error of the mass for each method used and the error as a function of the age, distance and extinction A_V . The results indicate that the mass error tends to increase with cluster age, distance and extinction being usually under 20%. This behavior is expected since more distant and old open clusters present a low sampling of the main-sequence stars and suffer from larger photometric uncertainties. There is also a small systematic overestimation of the mass by the integrated mass function method and a small underestimation in the detailed mass function method. Since it is computationally difficult to obtain individual mass error estimates for each cluster studied, we will adopt the conservative 20% value overall as our uncertainty in this work.

3 PLEIADES: A BENCHMARK CLUSTER

With the method tested and validated in a large grid of synthetic clusters, we proceeded to apply it to the Pleiades cluster, which can be considered a benchmark case since there are several studies on its stellar population and precise astrometric and photometric data. These data, especially from the *Gaia* catalogue, have allowed a precise determination of member stars and features in the cluster CMD. We took the sample of 1236 astrometric members, determined individual masses and applied the two methods described in the previous section to determine the cluster mass.

We compared our individual mass estimates with the determination of [Anders et al. \(2022\)](#), which used *Gaia eDR3*, Pan-STARRS1, SkyMapper, 2MASS, and AllWISE photometric data. Although estimating the mass was not their main goal, they provide the values which we compare to our estimates in Fig. 7, where it is possible to see a general good agreement but also a systematic deviation in the

binary stars. It is important to point out that their method assumes stars are single, so the values estimated are relative to the star that dominates the photometry, usually the primary. This fact may explain the systematic underestimation of the primary mass value seen in their method.

Masses from [Gaia Collaboration et al. \(2022\)](#) in data release DR3 were also available, and a comparison of the stars in common to our Pleiades member sample is shown in Fig. 7. As in the previous case, we can see that our results are in good agreement, especially single stars with masses lower than $\sim 2M_\odot$. There are again some disagreements regarding the masses of the primary stars in binary systems, as *Gaia* does not estimate the mass of the secondary stars in possible binary systems. However, here we see better agreement with our results with no clear systematic deviations.

As an example of individual mass estimate quality, in the observed stars, we found a mass of $4.94M_\odot$ for the *20Tauri* star. The mass of this star determined by our method agrees with other values found in the literature, such as $4.22M_\odot$ from [Zorec et al. \(2009\)](#), $4.29M_\odot$ from [Bodensteiner et al. \(2018\)](#) and $4.90M_\odot$ from [Kyritsis et al. \(2022\)](#).

It is also possible to check the consistency of the binary fraction estimated by our method. From the sample of the Pleiades member stars we identified, 1006 single stars and 230 binary systems, giving a binary fraction of 19%. The binary fraction estimates found published in the literature ranges from 17% to 50% with many works focusing on the lower mass population ([Stauffer 1982](#); [Steele & Jameson 1995](#); [Martín et al. 2003](#); [Lodieu et al. 2007](#); [Pinfield et al. 2003](#); [Maxted & Jeffries 2005](#); [Bate et al. 2002](#)). One of the first works to analyse the frequency of binaries in the Pleiades was [Bettis \(1975\)](#), which found a 22% binary fraction for main sequence stars. Recently, [Torres \(2020\)](#) found a fraction of multiple and binary systems of 37% (12/32), considering a list of 32 stars of spectral type B and A with data from *Gaia DR2*. A study of spectroscopic monitoring [Torres et al. \(2021\)](#) found a fraction of 17% (48/289) which, after corrections for incompleteness, took on a value of $(25 \pm 3)\%$. Our binary fraction estimate is within the reported range and should be considered as a lower limit since the contamination of false positive detection of members in the low magnitude interval ($G > 16$) may be significant.

From the masses of the primary and secondary stars of a binary system, we were able to calculate the average mass ratio in binary systems. For the binary stars of Pleiades, we found an average mass ratio of $q = M_{\text{secondary}}/M_{\text{primary}} = (0.58 \pm 0.23)$. This value is close to that found by [Malofeva et al. \(2022\)](#), who determined (0.73 ± 0.03) .

Applying the two methods described in the previous section, we proceed to obtain the mass of the cluster. From the observed stars we obtain the observed mass and for the unseen stars, we use the mass functions to estimate the unseen mass. In Fig. 8 we show the present-day mass function obtained from the observed member stars, excluding companion masses as detailed previously for the first method to obtain the mass. From this method, we obtained a mass of $(816 \pm 165)M_\odot$. For the second method, we used the mass functions shown in Fig. 9 where we show the present-day mass functions for single, primary and secondary stars as identified by our method. We performed segmented linear fits for each present-day mass function, where we obtained the slopes and transition mass points for the single, primary and secondary star populations. The results are presented in Table 1. From the fits, we obtain the slopes and transition mass points for the single star population which were: $\alpha_A = (-1.99 \pm 0.50)$, $\alpha_B = (0.03 \pm 0.24)$ and $M_C = (-0.20 \pm 0.07)$; for primary stars which were $\alpha_A = (-1.91 \pm 0.20)$, $\alpha_B = (0.01 \pm 0.48)$ and $M_C = (0.20 \pm 0.23)$; and for the secondary stars which were $\alpha_A = (-2.73 \pm 0.55)$, $\alpha_B = (0.28 \pm 0.23)$ and $M_C = (-0.12 \pm 0.05)$. We can see from the

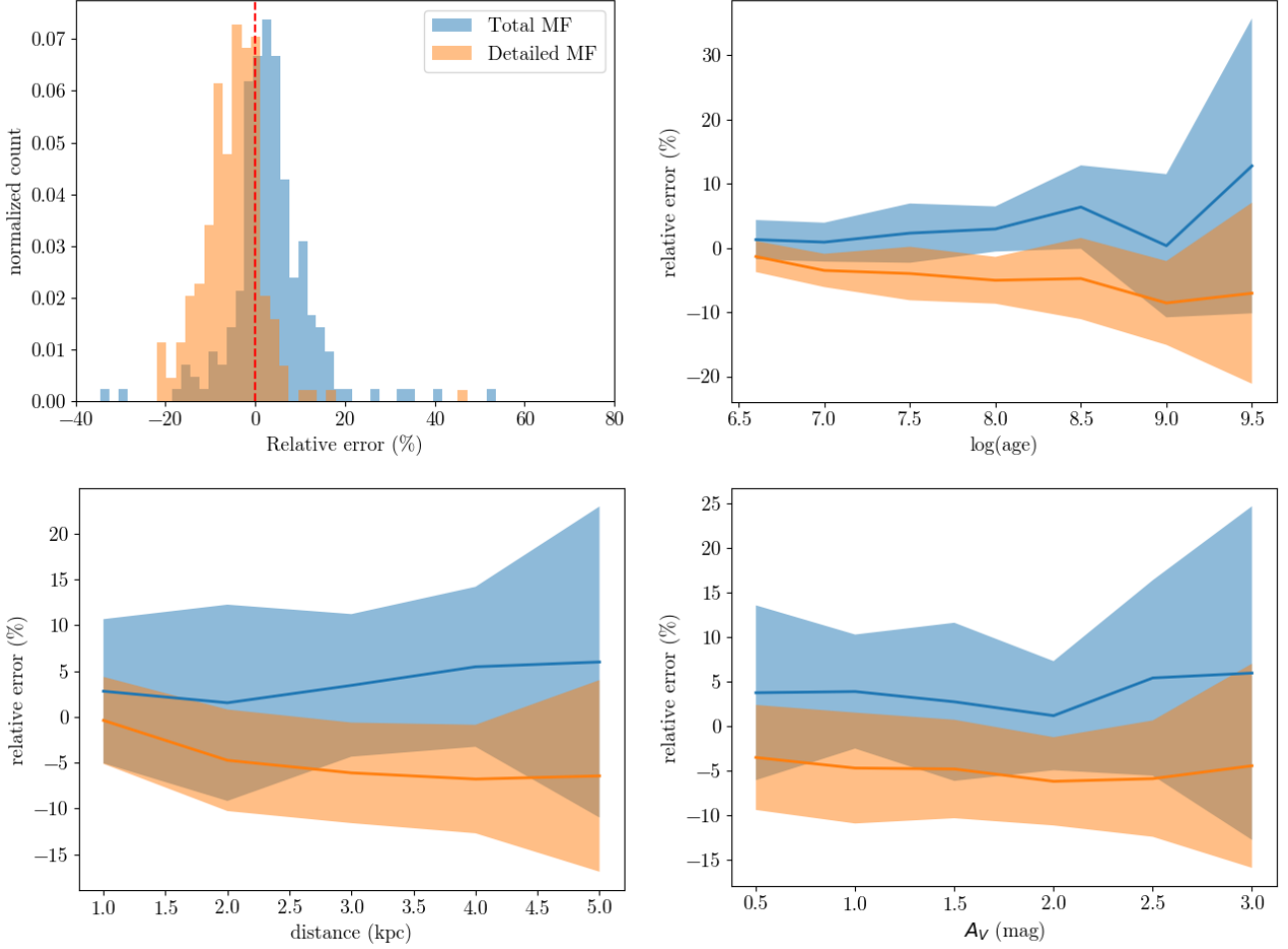


Figure 6. Distribution of the relative error on the cluster’s mass obtained for each method used (upper left), average relative error and the respective 1σ uncertainty as a function of $\log(\text{age})$ (upper right), distance (lower left) and A_V (lower right).

Table 1. Parameters of the segmented linear fits obtained for the distinct populations of the Pleiades member stars, present-day mass functions.

	Parameters		
	Low mass	Transition mass	High mass
Single	0.03 ± 0.24	-0.20 ± 0.07	-1.99 ± 0.50
Primary	0.01 ± 0.48	0.20 ± 0.23	-1.91 ± 2.19
Secondary	0.28 ± 0.23	-0.12 ± 0.05	-2.73 ± 0.55

results that in general, the slopes for the distinct sections of the mass function agree within the uncertainties obtained. The only exception is the high mass slope of the secondary star population, which is steeper than the others. From these values, we obtain the mass of the cluster using the detailed mass function as described in Sec. 2.2, with a value of $(847 \pm 169)M_{\odot}$.

A summary of our results, with a comparison to other values in the literature, is shown in Table 2 where the distinct methods used to estimate the masses are specified. We note that our results show general agreement with other authors, except for the value obtained by Raboud & Mermilliod (1997) which used the tidal radius to estimate the mass.

Table 2. Comparison of the mass of Pleiades with the results found in the literature. In the first line, we include the two values determined by us, $(816 \pm 36)M_{\odot}$ resulting from the integrated mass function and $(838 \pm 21)M_{\odot}$ from the detailed mass function (MF).

Reference	$M_T (m_{\odot})$	Method
This work	816 ± 165	integrated MF
	847 ± 169	detailed MF
Raboud & Mermilliod (1997)	1400	Tidal radius
	720	Virial
	950	integrated MF
Pinfield et al. (1998)	735	King profile
Adams et al. (2001)	800	King profile
Converse & Stahler (2008)	870 ± 34	integrated MF
Gao (2019)	721 ± 93	King profile
Danilov & Seleznev (2020)	855 ± 104	integrated MF
Ebrahimi et al. (2022)	807 ± 1	integrated MF

4 MASS OF REAL CLUSTERS

In this section, we present the results obtained in our analysis of masses of real open clusters. We have investigated a sample of 1743 open clusters from Dias et al. (2021) for which results of individual stellar membership probabilities as well as fundamental parameters such as age, distance, and extinction were available. For this sample, we updated the memberships and fundamental parameters using data

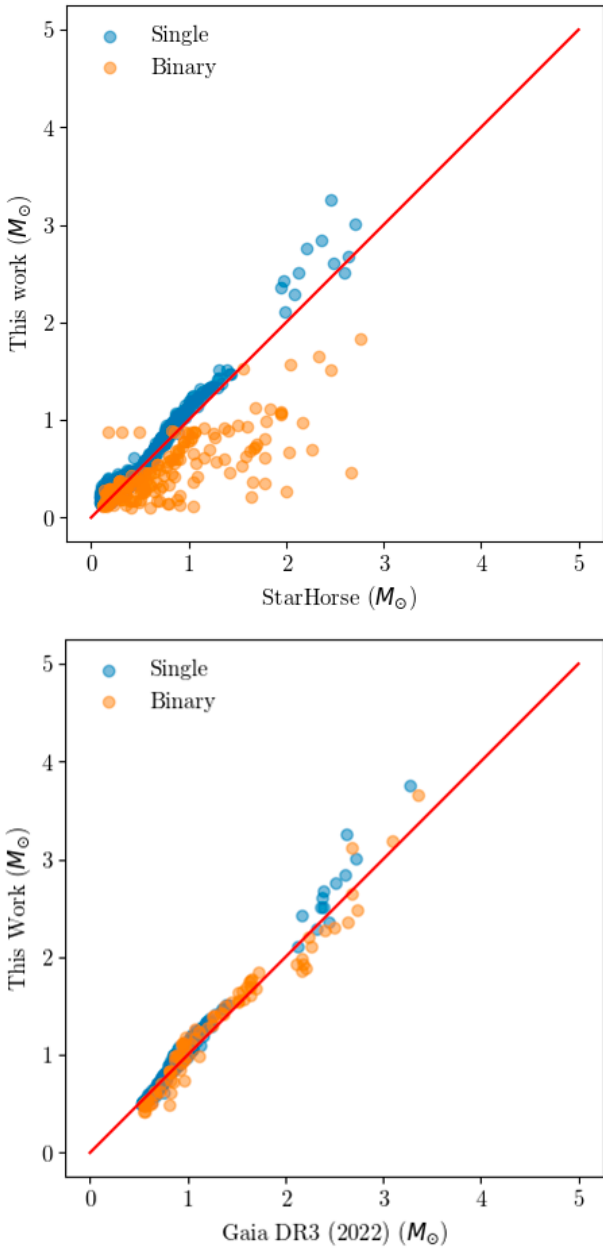


Figure 7. Comparison of individual stellar mass results from our work with [Anders et al. \(2022\)](#) (upper panel) and [Gaia Collaboration et al. \(2022\)](#) (lower panel). For the stars in binary systems the mass shown is that of the primary.

from the *Gaia* *eDR3* catalogue and obtained the present-day mass functions using the two methods presented in Section 2.2.

As mentioned before, the final sample was defined with clusters for which the present-day mass function had at least 2 bins on both sides of the transition mass point, a criterion that is sufficient to perform a fit with a straight line. Also, clusters that had visually high star contamination were removed. With this, we were able to obtain the mass for 773 clusters using the integrated mass function and 46 using the detailed mass function. Using this final sample, we investigated relationships with other parameters such as age and size, and location in the Galaxy, among others.

In Table 3, we present an example of the final sample and the

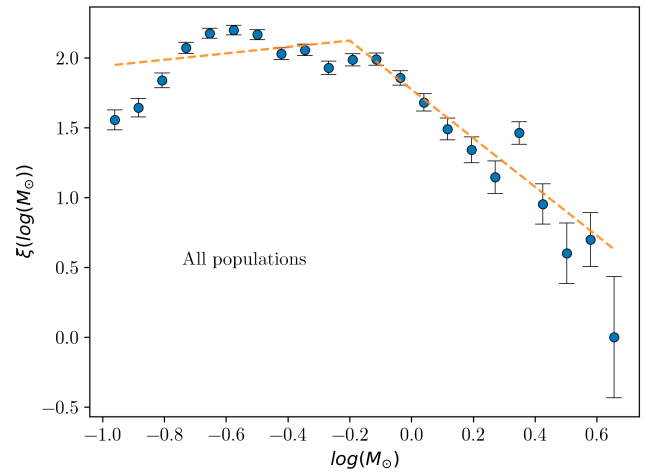


Figure 8. Pleiades integrated mass function results for the sample that includes all star populations. The slopes and transition mass point are $\alpha_A = (-1.75 \pm 0.33)$, $\alpha_B = (0.23 \pm 0.22)$ and $M_c = (-0.20 \pm 0.07)$.

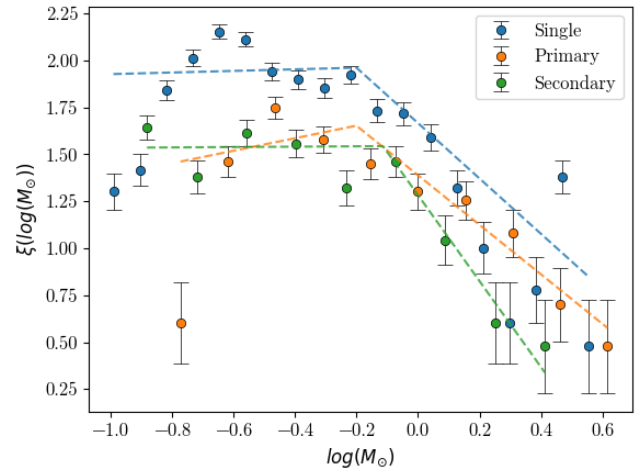


Figure 9. Pleiades present-day mass functions for single, primary and secondary stars. The slopes and transition mass points for the single star population are $\alpha_A = (-1.99 \pm 0.50)$, $\alpha_B = (0.03 \pm 0.24)$ and $M_c = (-0.20 \pm 0.07)$, for primary stars $\alpha_A = (-1.91 \pm 2.20)$, $\alpha_B = (0.01 \pm 0.48)$ and $M_c = (0.20 \pm 0.23)$ and the secondary stars $\alpha_A = (-2.73 \pm 0.55)$, $\alpha_B = (0.28 \pm 0.23)$ and $M_c = (-0.12 \pm 0.05)$.

masses determined for each cluster, as well as the fundamental parameters adopted for each. The full table is available online.

4.1 Comparison with literature

We compared our results of mass of the clusters with those of the large scale published in the literature, briefly summarized as follows and presented in Fig. 10.

We found 102 common objects with [Piskunov et al. \(2008a\)](#), which determined the mass using the King profile. Many objects show significant discrepancies in relation to our results. We find only 30 clusters for which the masses are relatively close to ours, with many objects showing significant discrepancies in relation to our results. The mean of the relative difference between our results was 193% and

Table 3. Sample table of fundamental parameters and masses determined for the open cluster sample using the two methods described in the text. The full table is available online.

Name	log(age)	Dist. (kpc)	Av. (mag.)	Fe/H	$M_{Tint}(m_{\odot})$	$M_{Tdet}(m_{\odot})$
ASCC 10	8.29 ± 0.09	0.642 ± 0.003	0.8 ± 0.1	0.004 ± 0.028	229 ± 45	
ASCC 105	8.12 ± 0.05	0.552 ± 0.002	0.8 ± 0.0	0.252 ± 0.066	304 ± 60	
ASCC 107	7.65 ± 0.36	0.847 ± 0.008	1.5 ± 0.2	0.253 ± 0.187	409 ± 81	
ASCC 108	8.24 ± 0.07	1.157 ± 0.003	0.7 ± 0.0	0.097 ± 0.033	935 ± 187	
ASCC 11	8.44 ± 0.19	0.826 ± 0.005	1.0 ± 0.1	0.121 ± 0.044	529 ± 105	541 ± 108

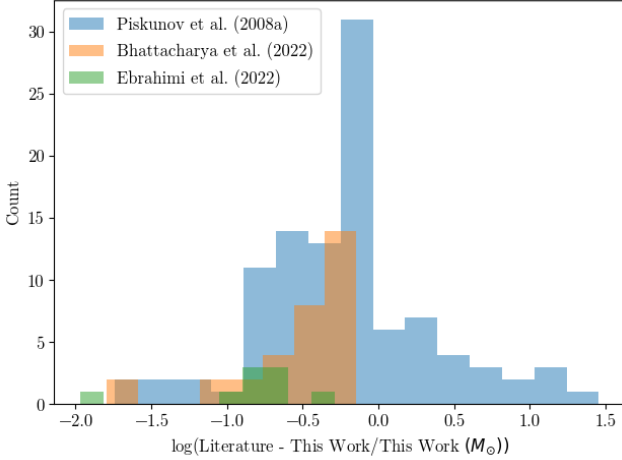


Figure 10. Relative error histogram comparing the masses of clusters in common with Piskunov et al. (2008a), Bhattacharya et al. (2022) and Ebrahimi et al. (2022).

the standard deviation was 380%. The differences can be explained by the different samples of member stars, as well as the different parameters (mainly distance and age) adopted for each cluster.

From the work Bhattacharya et al. (2022) we found 32 clusters in common which are presented in the histogram of relative errors, as shown in Fig. 10. Most clusters are within 60% of our masses, with a mean relative error of about 35% and a standard deviation of 20%. The differences observed are likely due to membership probabilities and fundamental parameters adopted by the authors, which are distinct from the ones used in this work.

For Bukowiecki et al. (2012), which had determination of masses for 599 open clusters, we were not able to find a complete table with the masses for comparison to our results.

The work of Ebrahimi et al. (2022) determined the mass of the Pleiades, which is close to the one found by us (see Table 2). For the other clusters of the work, we found 9 in common and 6 of these are close to our values with a relative error of approximately 15% - 30%. Again, differences are likely due to membership probabilities and fundamental parameters adopted by the authors, which are distinct from the ones adopted in this work.

Also, worthy of note, Bonatto & Bica (2005) estimated masses from mass functions obtained using 2MASS photometry. We found 4 clusters in common to their sample and, in general, our results give larger masses with some values agreeing within the uncertainties. For NGC 6694 the authors estimated $(1900 \pm 700)M_{\odot}$ and we obtained $(1208 \pm 242)M_{\odot}$ using integrated mass function method; for NGC 2287 the authors found $(720 \pm 90)M_{\odot}$ and we find $(1185 \pm 237)M_{\odot}$ from the methods detailed mass function and $(1126 \pm 225)M_{\odot}$ integrated MF, respectively; for NGC 2548 and authors estimated a mass of $(630 \pm 150)M_{\odot}$ and our results are $(912 \pm 182)M_{\odot}$ using detailed

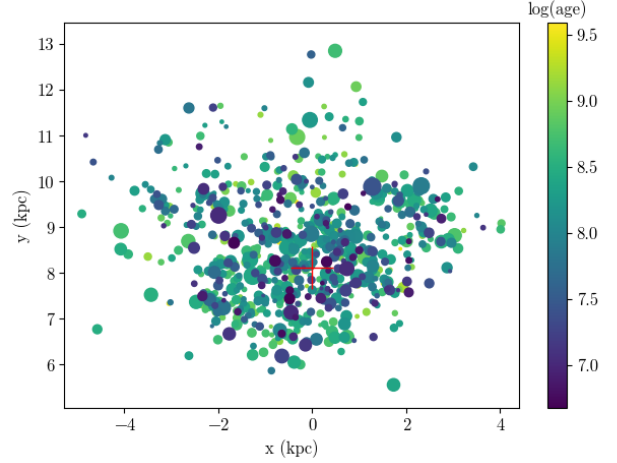


Figure 11. Distribution of the 773 open clusters in the galactic plane, with their masses determined using the mass function integrated. The Sun is referenced with a red cross at coordinates (0, 8.3) kpc and the galactic centre is at (0,0). The vector angular velocity is perpendicular to the x-y plane, pointing in the direction of the paper. The size of the dots is proportional to the mass.

mass function and $(920 \pm 184)M_{\odot}$ using integrated MF. Finally, for the case of NGC 2682, a mass of $(990 \pm 120)M_{\odot}$ was found by the authors and $(1843 \pm 369)M_{\odot}$ according to our results from integrated mass function method.

Finally, some works have mass estimates for isolated clusters. In the work of Yalyalieva et al. (2022) two estimates of masses using isochrones fits for NGC 225 were obtained: 1) $(155.2 \pm 2.0)M_{\odot}$ up to magnitude G of 18 of Gaia EDR3 and assuming a binary fraction of zero; 2) $(170.5 \pm 2.2)M_{\odot}$ with a binary fraction of 0.52. Our results for the integrated mass function returned a mass of $(124 \pm 5)M_{\odot}$ and a fraction of 0.62 binary stars. In Bai et al. (2022) the authors found $439M_{\odot}$ for COIN-Gaia 13 using the integration of the mass function of the observed stars disregarding the influence of binary stars. Regarding this cluster our result was $(367 \pm 9)M_{\odot}$ for detailed mass function and $(378 \pm 16)M_{\odot}$ for integrated MF, we also found a fraction of 0.60 of binaries which can explain part of the difference in masses found.

4.2 Mass properties of the sample

The large number of masses of the open clusters determined in this study allowed us to investigate the relation of this parameter with others such as age, radius, and mass segregation, for example. We start by looking at the distribution of open clusters in the Galactic plane, as shown in Fig. 11. In the figure, the size of the dots is proportional to the mass and no clear pattern of the distribution of massive clusters is seen.

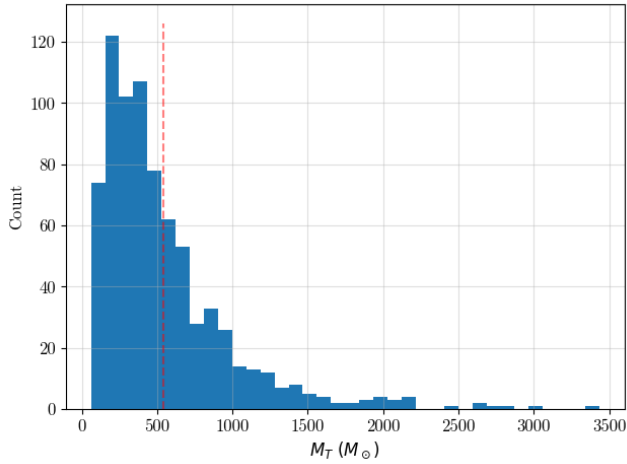


Figure 12. Histogram of the mass distribution of clusters in the integrated mass function sample. The vertical line in red indicates the mean of the distribution.

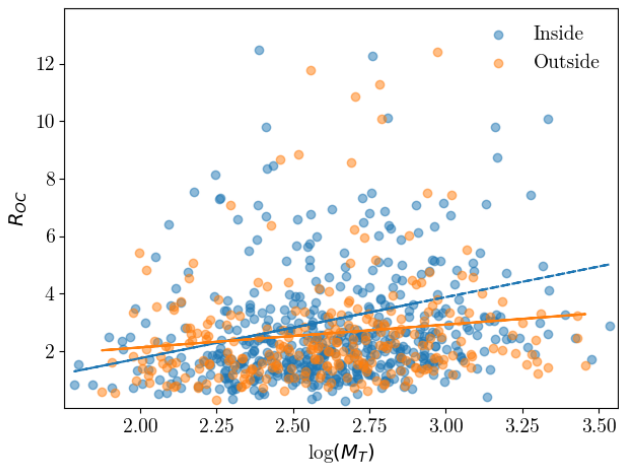


Figure 13. Mass-radius distribution for the clusters in the sample of 773 open clusters, with their masses determined by the integrated mass function. The blue dots represent the clusters within the solar orbit, while the orange dots represent the clusters outside the solar orbit. The lines represent the linear fits for the inner and outer orbit samples, respectively.

In Fig. 12 we show the distribution of cluster masses for our sample. The weighted mean of this distribution is $544M_{\odot}$ with a standard deviation of $447M_{\odot}$.

In the work by Joshi et al. (2016), the authors investigated the relation of the radius and age of the cluster to the mass. The idea is that the mass-radius relationship gives information on the dynamic evolution of the open cluster since, during their early evolution, clusters are expected to experience interactions with massive molecular clouds which can lead to mass loss and a reduction in size. In Fig. 13 we show the results we find for the mass and cluster radius relationship. The radii of the clusters adopted are defined as the value that includes 50% of the stars in the system. For clusters inside the solar orbit we find the correlation $R_{OC} = (2.13 \pm 1.07)\log(M_T) - (2.51 \pm 2.83)$ and for clusters out-

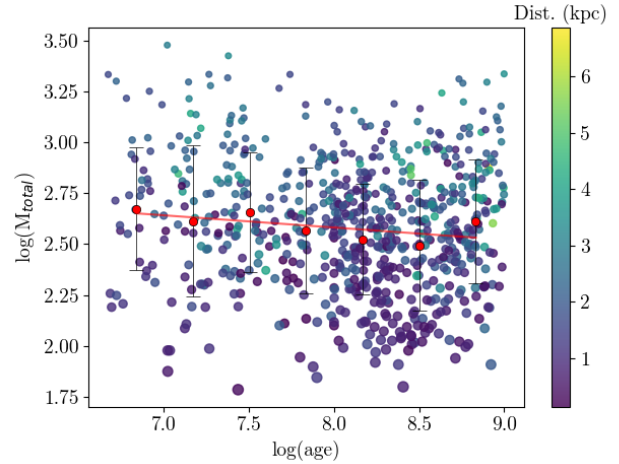


Figure 14. Relation of cluster mass to age with red dots representing the average of the masses in a bin in an interval of $\log(\text{age}) = 0.3$. Error bars are obtained from the standard deviation of the bin sample.

side the solar orbit $R_{OC} = (0.80 \pm 0.96)\log(M_T) + (0.53 \pm 0.96)$. Our results are in agreement with those obtained by Joshi et al. (2016), where we find few massive clusters with smaller radii as well as a lack of low-mass clusters with large radii. We also see that clusters inside the solar orbit show a steeper correlation, which can be an indication that massive clusters with larger radii have a lower chance of surviving interactions in the direction of the Galactic centre. However, given the uncertainties in the linear fits, the difference is not significant, which is likely due to the large data dispersion.

We have also investigated the mass-age relation for our cluster sample, as shown in Fig. 14. Here the general expectation is that interactions with the Galactic tidal field or with the molecular clouds affect their structure and a trend where mass decreases with age should be seen. In our sample, a very tenuous relation is seen, with a correlation coefficient of -0.1, which is considerably lower than the value of -0.95 found by Joshi et al. (2016). If we take the average of the mass in intervals of $\log(\text{age})$ in the same manner as done by Joshi et al. (2016), excluding clusters with ages greater than $\log(\text{age}) = 9.0$ to avoid introducing a selection effect bias, we obtain the following correlation: $\log(M_T) = (-0.06 \pm 0.03)\log(\text{age}) + (3.06 \pm 0.24)$. As in Joshi et al. (2016), we see in our results that younger clusters tend to have higher mass and lose mass as they get older, but the effect is significantly smaller. In Joshi et al. (2016) the authors found a slope of -0.36 and a mass loss rate $dM_{\odot}/d(\text{age}) = 150M_{\odot}$ for the age range 1-10 Myr. In our results we find a mass loss, with a slope of -0.06, that is less intense and a rate of $dM_{\odot}/d(\text{age}) = 13M_{\odot}$ for clusters in the age interval of 1-10 Myr. Here we also performed a LOWESS regression and inspected the uncertainties, finding that a small effect is present, but it is not significant.

We have also measured the degree of mass segregation within the clusters. To do this, we separate the member stars of a given cluster into two groups: one having members with masses $> 1M_{\odot}$ and the other with $< 1M_{\odot}$. With these groups, we use two distinct procedures to measure the degree of mass segregation. One, using the ratio of the mean radius of each group's distribution, and the other, using a comparison of the cumulative distribution of mass with respect to the radius, similar to the one used by Mužić et al. (2022), where they were concerned in determining whether there was or not mass segregation. Unlike that work, here we quantify the effect

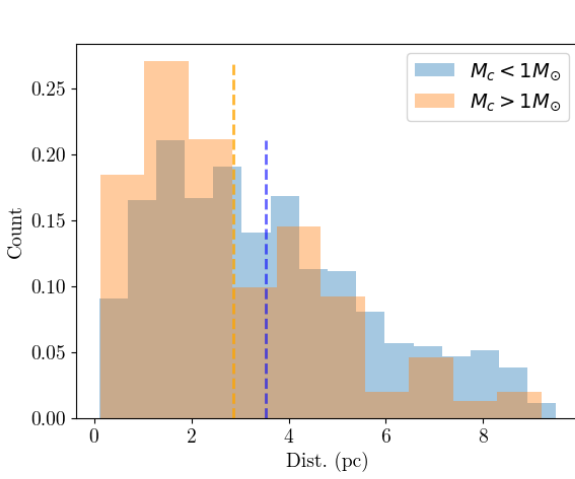


Figure 15. Mass segregation for Pleiades, using the distribution of star counts as a function of radius. The member stars were divided into two groups, one with masses $> 1M_\odot$ and one with $< 1M_\odot$. The vertical line in orange represents the mean radius of mass concentration for stars $> 1M_\odot$ and in blue the mean radius for stars $< 1M_\odot$.

using the Kolmogorov-Smirnov measure to quantify the difference between the distributions. As an example, in Fig. 15 we show the distributions of the two groups as obtained for the Pleiades cluster. In the figure, the difference in the mean radius of each group is indicated and the distinction is clear. Our results corroborate the existence of mass segregation, which was also established by van Leeuwen et al. (1986), Hambly et al. (1995), and Raboud & Mermillod (1998a) for this cluster.

For the second method, we could determine the significance level of the Kolmogorov-Smirnov measure, indicating how reliable the measured differences between the high and low mass distributions were. With the significance test (p-value) and the adopted threshold of significance of 0.05, we defined a subsample of clusters for which $p\text{-value} < 0.05$. We found that in our sample, 368 (48%) open clusters had a significant level of mass segregation.

With the mass segregation measure obtained using the two methods, we looked at how it related to the ages of the clusters in our sample. In Fig. 16 we show the results for this relation where there is no clear trend in the relation of mass segregation with age. The trend line is obtained with a LOWESS regression procedure where the uncertainties were also estimated, and the sample mean of each segregation statistic is also presented for comparison. In the first panel, we show the result using the first method, based on the ratio of the mean radius of the low mass sample ($\overline{R_{lm}}$) to the mean radius of the high mass sample ($\overline{R_{hm}}$). We see the same behavior for the second method to estimate mass segregation, shown in the second panel of the figure, where the Kolmogorov-Smirnov measure was used. No significant difference between the two methods, as far as the existence of the correlation, is seen. Some authors have mentioned the possibility that low-mass members would tend to escape as the cluster evolves and moves towards a relaxation state. However, we do not detect evidence for that here.

We also investigated other possible correlations with cluster properties, looking at parameters such as the metallicity, cluster radius, cluster stellar density and cluster mass. We also investigated the subsample based on the significance level of the Kolmogorov-Smirnov measure, taking only those clusters for which the distributions showed

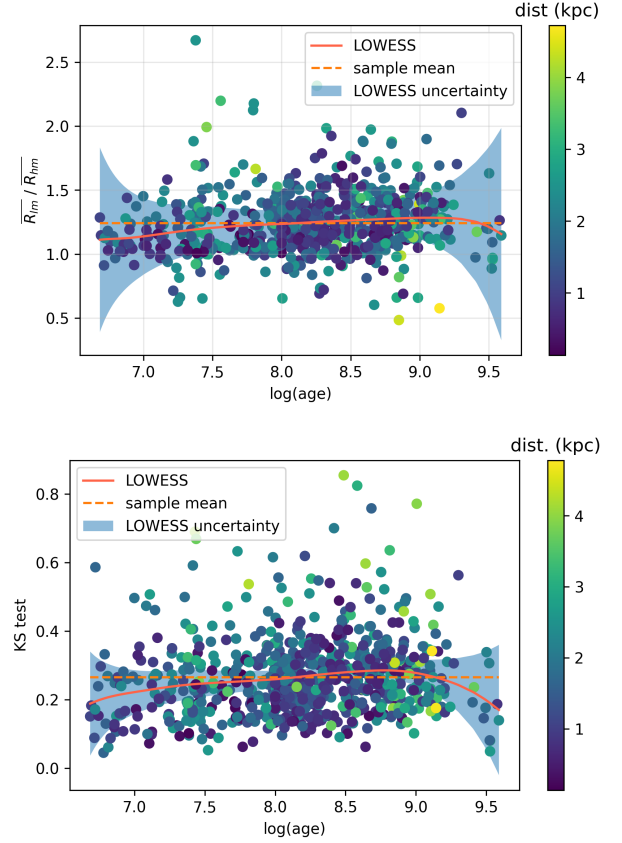


Figure 16. Relation of mass segregation to log(age), as measured by the ratio of mean radius for high and low mass groups (upper panel) and Kolmogorov-Smirnov measure (lower panel). The tendency line (red) obtained by LOWESS regression and its uncertainty, as well as the sample mean, is also shown.

differences with a p-value lower than 0.05. The only parameter for which a significant correlation was observed was cluster mass. The correlation for this parameter using the high significance sub-sample is shown in Fig. 17 where a trend line based on a LOWESS regression is shown with its respective uncertainty.

It is important to note that there is no consensus as to which method to measure mass segregation is ideal. As mentioned in Mužić et al. (2022), methods which were considered ideal by Parker & Goodwin (2015), who compared four different methods which are used to measure mass segregation, were not effective for the clusters they studied. However, both methods adopted in our work give results that agree with each other and, at least statistically in the context of our sample, indicate that mass segregation does not increase with age as has been suggested by other authors.

5 CONCLUSIONS

In this work, we present a new method for determining individual stellar masses and use it to calculate the masses for a sample of 773 open clusters from the Dias et al. (2021) catalog, with updated memberships and fundamental parameters based on astrometric and photometric data from *Gaia* eDR3.

The method for determining individual masses uses high-quality

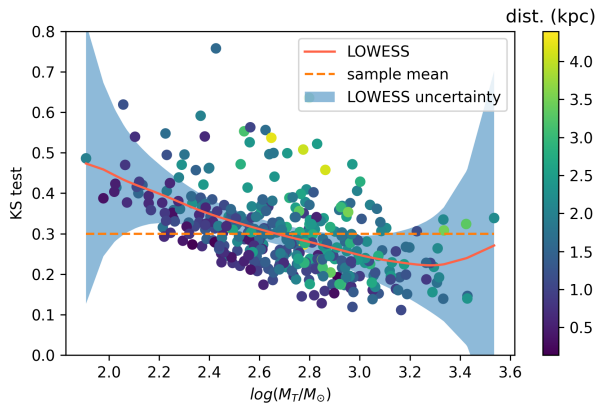


Figure 17. Relation of mass segregation, obtained by Kolmogorov-Smirnov measure, to cluster mass for the subsample with the significance level of $p < 0.05$. The tendency line (red) obtained by LOWESS regression and its uncertainty, as well as the sample mean is also shown.

data of the member stars and fundamental parameters of open clusters, to compare to synthetic clusters generated with full control of relevant parameters, and a Monte-Carlo method to obtain the individual masses and assess its uncertainties and limitations. The masses are estimated by comparing the observed stars with synthetic stars generated in a Monte-Carlo method, finding the nearest star in magnitude space, assigning it a mass, and marking it as binary if applicable. The method was validated with a synthetic cluster grid, and the results were found to be in good agreement with the input masses. Some limitations include difficulty in detecting binary stars in specific regions of the CMD where the main sequence and binary regions overlap, leading to incorrect mass estimation in some cases.

With the individual stellar masses estimated, we determined the mass of the star clusters using two integration methods. In the first method, we integrated the mass function, which contains all the stars in the cluster, a method often used in the literature, and in the second method we performed a detailed integration, which considers a mass function for each population of stars within the cluster (individual, primary and secondary). The unobserved mass was estimated by extrapolating the mass function of the observed stars and accounting for evolved stars and low-mass stars. The method involves obtaining the mass function of the observed star masses and fitting a two-part segmented linear function to it. The contribution of binary systems is estimated by obtaining the mean mass fraction for binary systems and multiplying that value by the estimated mass of single stars when using the integration of the mass function and in detail when using specific population mass functions of the detailed integration method. The method is validated by applying it to a grid of synthetic clusters and comparing the results with the true masses. The results show that we can recover masses with uncertainties under 20% in most cases, and thus this is the value we adopted as a conservative error estimate.

We applied our methodology to the observed clusters first examining in detail the results for the well-known Pleiades open cluster. The individual masses we estimate for the member stars of this cluster are in agreement with the masses of [Gaia Collaboration et al. \(2022\)](#) and the StarHorse catalogue ([Anders et al. 2022](#)). The mass obtained for Pleiades using the two methods, the binary fraction and the average

mass ratio of binary systems, showed good agreement with other results found in the literature.

The comparison of our mass estimates of the open clusters to other works in the literature shows good agreement with recent works based on *Gaia* data but large discrepancies with the works of pre-*Gaia* catalogues. Large discrepancies were seen when comparing to the work of [Piskunov et al. \(2008a\)](#) who determined masses using the tidal radius, determined from the cluster structural parameters.

After the thorough validation of the procedures, we focused on the relationship between the mass, cluster radius, and age. The results indicate that the effect seen by [Joshi et al. \(2016\)](#), that younger clusters tend to have higher mass and lose mass as they get older, is not significant in our sample. We find a mass loss rate of $13M_{\odot}/\text{Myr}$ which is significantly lower than the value found by those authors. We find that the correlation between cluster mass and age is weak, with a correlation coefficient of -0.1 . The discrepancies in the results are likely due to differences in the samples, memberships and fundamental parameters used.

Looking at the relationship between clusters' masses and radii, we find few massive clusters with smaller radius as well as a lack of low-mass clusters with large radius. The positive correlation between mass and cluster radius could be an indication that clusters inside the solar orbit have a lower chance of surviving interactions in the region of the Galactic centre, however, the difference is not significant. We also looked at the degree of mass segregation within the clusters by measuring it using two distinct methods and found that 368 (48%) open clusters show a significant level of mass segregation. However, we found no clear significant trend in the relation of mass segregation with age, cluster density, or radius. We did however find a relation between the cluster mass and segregation, showing that more massive clusters tend to be less segregated. Regarding mass segregation, our results are in agreement with [Dib et al. \(2018\)](#), where no significant relation of mass segregation to age was found.

ACKNOWLEDGEMENTS

Wilton Dias would like to thank CNPq grant 310765/2020-0. Hektor Monteiro would like to thank CNPq grant 436117/2018-5 and FAPEMIG grant APQ 01305-17. This work has made use of the computing facilities available at the Laboratory of Computational Astrophysics of the Universidade Federal de Itajubá (LAC-UNIFEI). The LAC-UNIFEI is maintained with grants from CAPES, CNPq and FAPEMIG.

DATA AVAILABILITY

The data underlying this article, that support the plots and other findings, are available in the article and in its online supplementary material (<https://ocmass.streamlit.app>). The updated memberships and individual stellar masses and any other data relevant to the results presented here will be made available upon reasonable requests.

This work has made use of data from the European Space Agency (ESA) *Gaia* (<http://www.cosmos.esa.int/Gaia>) mission, processed by the *Gaia* Data Processing and Analysis Consortium (DPAC, <http://www.cosmos.esa.int/web/Gaia/dpac/consortium>).

We also employed catalogs from CDS/Simbad (Strasbourg) and Digitized Sky Survey images from the Space Telescope Science Institute (US Government grant NAG W-2166)

REFERENCES

- Adams J. D., Stauffer J. R., Monet D. G., Skrutskie M. F., Beichman C. A., 2001, *AJ*, **121**, 2053
- Anders F., et al., 2022, *A&A*, **658**, A91
- Bai L., Zhong J., Chen L., Li J., Hou J., 2022, *Research in Astronomy and Astrophysics*, **22**, 055022
- Bate M. R., Bonnell I. A., Bromm V., 2002, *MNRAS*, **332**, L65
- Bettis C., 1975, *PASP*, **87**, 707
- Bhattacharya S., Rao K. K., Agarwal M., Balan S., Vaidya K., 2022, *MNRAS*, **517**, 3525
- Bisht D., Zhu Q., Yadav R. K. S., Durgapal A., Rangwal G., 2020, *MNRAS*, **494**, 607
- Bodensteiner J., Baade D., Greiner J., Langer N., 2018, *A&A*, **618**, A110
- Bonatto C., Bica E., 2005, *A&A*, **437**, 483
- Bressan A., Marigo P., Girardi L., Salasnich B., Dal Cero C., Rubele S., Nanni A., 2012, *MNRAS*, **427**, 127
- Bukowiecki L., Maciejewski G., Konorski P., Niedzielski A., 2012, *Acta Astron.*, **62**, 281
- Cantat-Gaudin T., 2022, *Universe*, **8**, 111
- Chabrier G., 2003, *PASP*, **115**, 763
- Converse J. M., Stahler S. W., 2008, *ApJ*, **678**, 431
- Cummings J. D., Kalirai J. S., Tremblay P. E., Ramirez-Ruiz E., Choi J., 2018, *ApJ*, **866**, 21
- Danilov V. M., Seleznev A. F., 2020, *Astrophysical Bulletin*, **75**, 407
- Dias W. S., Monteiro H., Moitinho A., Lépine J. R. D., Carraro G., Paunzen E., Alessi B., Vilella L., 2021, *MNRAS*, **504**, 356
- Dib S., Schmeja S., Parker R. J., 2018, *MNRAS*, **473**, 849
- Durgapal A. K., Pandey A. K., 2001, *A&A*, **375**, 840
- Ebrahimi H., Sollima A., Haghii H., 2022, *MNRAS*, **516**, 5637
- Gaia Collaboration et al., 2016, *A&A*, **595**, A1
- Gaia Collaboration Brown A. G. A., Vallenari A., Prusti T., de Bruijne J. H. J., Babusiaux C., Bailer-Jones C. A. L., 2018, preprint, ([arXiv:1804.09365](https://arxiv.org/abs/1804.09365))
- Gaia Collaboration et al., 2021, *A&A*, **649**, A1
- Gaia Collaboration et al., 2022, arXiv e-prints, [p. arXiv:2208.00211](https://arxiv.org/abs/2208.00211)
- Gao X.-h., 2019, *PASP*, **131**, 044101
- Goodwin S. P., Bastian N., 2006, *MNRAS*, **373**, 752
- Hambly N. C., Steele I. A., Hawkins M. R. S., Jameson R. F., 1995, *Monthly Notices of the Royal Astronomical Society*, **273**, 505
- Hetem A., Gregorio-Hetem J., 2019, *MNRAS*, **490**, 2521
- Joshi Y. C., Dambis A. K., Pandey A. K., Joshi S., 2016, *A&A*, **593**, A116
- Kharchenko N. V., Scholz R. D., Piskunov A. E., Röser S., Schilbach E., 2007, *Astronomische Nachrichten*, **328**, 889
- Kharchenko N. V., Piskunov A. E., Schilbach E., Röser S., Scholz R. D., 2013a, *A&A*, **558**, A53
- Kharchenko N. V., Piskunov A. E., Schilbach E., Röser S., Scholz R. D., 2013b, *A&A*, **558**, A53
- King I., 1962, *AJ*, **67**, 471
- Krause M. G. H., et al., 2020, *Space Sci. Rev.*, **216**, 64
- Krumholz M. R., McKee C. F., Bland-Hawthorn J., 2019, *ARA&A*, **57**, 227
- Kyritsis E., Maravelias G., Zezas A., Bonfini P., Kovlakas K., Reig P., 2022, *A&A*, **657**, A62
- Lodieu N., Dobbie P. D., Deacon N. R., Hodgkin S. T., Hambly N. C., Jameson R. F., 2007, *MNRAS*, **380**, 712
- Malofeva A. A., Mikhnevich V. O., Carraro G., Seleznev A. F., 2022, arXiv e-prints, [p. arXiv:2211.12745](https://arxiv.org/abs/2211.12745)
- Martín E. L., y Navascués D. B., Baraffe I., Bouy H., Dahm S., 2003, *The Astrophysical Journal*, **594**, 525
- Maxted P. F. L., Jeffries R. D., 2005, *MNRAS*, **362**, L45
- McNamara B. J., Sanders W. L., 1983, *A&A*, **118**, 361
- Mužić K., Almendros-Abad V., Bouy H., Kubiak K., Peña Ramírez K., Krone-Martins A., Moitinho A., Conceição M., 2022, *A&A*, **668**, A19
- Pandey A. K., Mahra H. S., Sagar R., 1992, *Bulletin of the Astronomical Society of India*, **20**, 287
- Parker R. J., Goodwin S. P., 2015, *MNRAS*, **449**, 3381
- Pijlloo J. T., Portegies Zwart S. F., Alexander P. E. R., Gieles M., Larsen S. S., Groot P. J., Devecchi B., 2015, *MNRAS*, **453**, 605
- Pinfield D. J., Jameson R. F., Hodgkin S. T., 1998, *MNRAS*, **299**, 955
- Pinfield D. J., Dobbie P. D., Jameson R. F., Steele I. A., Jones H. R. A., Katsiyannis A. C., 2003, *MNRAS*, **342**, 1241
- Piskunov A. E., Schilbach E., Kharchenko N. V., Röser S., Scholz R. D., 2007, *A&A*, **468**, 151
- Piskunov A. E., Schilbach E., Kharchenko N. V., Röser S., Scholz R. D., 2008a, *A&A*, **477**, 165
- Piskunov A. E., Kharchenko N. V., Schilbach E., Röser S., Scholz R. D., Zinnecker H., 2008b, *A&A*, **487**, 557
- Portegies Zwart S. F., McMillan S. L. W., Gieles M., 2010, *ARA&A*, **48**, 431
- Raboud D., 1996, *VizieR Online Data Catalog*, [pp J/A+A/315/384](https://vizier.cesr.cnrs.fr/vizieR/obj/J/A+A/315/384)
- Raboud D., Mermilliod J.-C., 1997, arXiv preprint astro-ph/9708144
- Raboud D., Mermilliod J. C., 1998a, *A&A*, **329**, 101
- Raboud D., Mermilliod J. C., 1998b, *A&A*, **333**, 897
- Rangwal G., Yadav R. K. S., Durgapal A., Bisht D., Nardiello D., 2019, *MNRAS*, **490**, 1383
- Röser S., Schilbach E., Schwan H., Kharchenko N. V., Piskunov A. E., Scholz R. D., 2008, *A&A*, **488**, 401
- Rossi L. J., Bekki K., Hurley J. R., 2016, *MNRAS*, **462**, 2861
- Salpeter E. E., 1955, *ApJ*, **121**, 161
- Skrutskie M. F., et al., 2006, *AJ*, **131**, 1163
- Spitzer Lyman J., 1958, *ApJ*, **127**, 17
- Stauffer J. R., 1982, *AJ*, **87**, 1507
- Steele I. A., Jameson R. F., 1995, *MNRAS*, **272**, 630
- Sturges H. A., 1926, *Journal of the American Statistical Association*, **21**, 65
- Torres G., 2020, *ApJ*, **901**, 91
- Torres G., Latham D. W., Quinn S. N., 2021, *ApJ*, **921**, 117
- Yalyaliev L., Carraro G., Glushkova E., Munari U., Ochner P., 2022, *MNRAS*,
- Yontan T., et al., 2019, *Ap&SS*, **364**, 152
- Zorec J., Cidale L., Arias M. L., Frémat Y., Muratore M. F., Torres A. F., Martayan C., 2009, *A&A*, **501**, 297
- van Leeuwen F., Alphenaar P., Brand J., 1986, *A&AS*, **65**, 309
- van den Bergh S., Lafontaine A., 1984, *AJ*, **89**, 1822

APPENDIX A: ONLINE MATERIAL

If you want to present additional material which would interrupt the flow of the main paper, it can be placed in an Appendix which appears after the list of references.

Table A1: Fundamental parameters and masses integrated and detailed determined for the open cluster sample.

Name	log(age)	Dist. (kpc)	Av. (mag.)	Fe/H	$M_{Tint}(m_{\odot})$	$M_{Tdet}(m_{\odot})$
ASCC 10	8.292 ± 0.088	0.642 ± 0.003	0.793 ± 0.068	0.004 ± 0.028	229 ± 45	
ASCC 105	8.117 ± 0.053	0.552 ± 0.002	0.765 ± 0.006	0.252 ± 0.066	304 ± 60	
ASCC 107	7.652 ± 0.359	0.847 ± 0.008	1.463 ± 0.204	0.253 ± 0.187	409 ± 81	
ASCC 108	8.241 ± 0.071	1.157 ± 0.003	0.655 ± 0.050	0.097 ± 0.033	935 ± 187	
ASCC 11	8.443 ± 0.194	0.826 ± 0.005	0.975 ± 0.101	0.121 ± 0.044	529 ± 105	541 ± 108
ASCC 113	8.493 ± 0.088	0.558 ± 0.001	0.245 ± 0.049	0.001 ± 0.025	413 ± 82	426 ± 85
ASCC 114	8.103 ± 0.089	0.900 ± 0.006	1.208 ± 0.091	0.059 ± 0.055	432 ± 86	
ASCC 115	8.308 ± 0.187	0.747 ± 0.003	0.907 ± 0.090	0.049 ± 0.063	140 ± 28	
ASCC 12	8.496 ± 0.318	1.014 ± 0.012	1.009 ± 0.084	0.112 ± 0.033	359 ± 71	309 ± 61
ASCC 127	7.549 ± 0.107	0.332 ± 0.013	0.575 ± 0.055	0.005 ± 0.044	207 ± 41	
ASCC 128	8.388 ± 0.100	0.644 ± 0.001	0.681 ± 0.069	0.052 ± 0.055	241 ± 48	
ASCC 13	8.134 ± 0.053	1.080 ± 0.004	0.882 ± 0.049	0.120 ± 0.050	576 ± 115	
ASCC 16	7.301 ± 0.072	0.342 ± 0.001	0.038 ± 0.053	0.180 ± 0.019	441 ± 88	
ASCC 21	7.011 ± 0.035	0.339 ± 0.001	0.283 ± 0.065	0.118 ± 0.040	367 ± 73	
ASCC 23	8.489 ± 0.084	0.604 ± 0.001	0.376 ± 0.044	0.069 ± 0.046	248 ± 49	242 ± 48
ASCC 29	8.129 ± 0.085	0.988 ± 0.011	0.245 ± 0.023	0.077 ± 0.025	183 ± 36	
ASCC 30	8.284 ± 0.061	1.054 ± 0.014	0.662 ± 0.087	0.115 ± 0.066	325 ± 65	
ASCC 41	8.000 ± 0.001	0.292 ± 0.001	0.010 ± 0.001	0.036 ± 0.001	126 ± 25	
ASCC 67	7.933 ± 0.054	1.878 ± 0.051	0.826 ± 0.032	0.122 ± 0.062	869 ± 173	
ASCC 71	8.071 ± 0.045	1.236 ± 0.023	1.001 ± 0.065	0.069 ± 0.079	432 ± 86	
ASCC 77	8.162 ± 0.074	1.079 ± 0.012	0.824 ± 0.040	0.124 ± 0.036	480 ± 96	
ASCC 85	8.267 ± 0.090	0.847 ± 0.006	0.747 ± 0.026	0.056 ± 0.036	383 ± 76	
ASCC 9	7.265 ± 0.062	2.119 ± 0.050	2.579 ± 0.031	0.106 ± 0.079	2154 ± 430	
ASCC 97	8.070 ± 0.167	0.561 ± 0.003	1.508 ± 0.065	0.075 ± 0.080	280 ± 56	
Alessi 10	8.558 ± 0.093	0.434 ± 0.001	0.445 ± 0.033	0.049 ± 0.021	122 ± 24	
Alessi 12	8.369 ± 0.114	0.534 ± 0.001	0.272 ± 0.035	0.003 ± 0.019	485 ± 97	
Alessi 2	8.502 ± 0.034	0.602 ± 0.002	0.923 ± 0.058	0.086 ± 0.022	317 ± 63	
Alessi 21	8.000 ± 0.001	0.557 ± 0.001	0.372 ± 0.001	0.048 ± 0.001	386 ± 77	
Alessi 37	8.417 ± 0.127	0.698 ± 0.002	0.647 ± 0.061	0.009 ± 0.044	309 ± 61	
Alessi 6	8.624 ± 0.093	0.859 ± 0.007	1.225 ± 0.085	0.191 ± 0.044	598 ± 119	
Alessi 62	8.936 ± 0.014	0.607 ± 0.002	0.864 ± 0.094	0.035 ± 0.059	285 ± 57	
Alessi 8	8.320 ± 0.067	0.650 ± 0.003	0.335 ± 0.046	0.051 ± 0.054	163 ± 32	
Alessi Teutsch 11	8.253 ± 0.130	0.638 ± 0.002	0.257 ± 0.047	0.024 ± 0.039	217 ± 43	217 ± 43
Alessi Teutsch 3	8.173 ± 0.170	0.684 ± 0.002	0.744 ± 0.043	0.039 ± 0.020	235 ± 47	192 ± 38
Antalova 2	6.760 ± 0.073	1.184 ± 0.030	1.336 ± 0.118	0.019 ± 0.045	161 ± 32	
BDSB96	6.685 ± 0.055	1.083 ± 0.017	1.130 ± 0.240	0.003 ± 0.088	181 ± 36	
BH 164	7.769 ± 0.052	0.399 ± 0.007	0.422 ± 0.050	0.003 ± 0.021	432 ± 86	
BH 200	7.416 ± 0.065	2.038 ± 0.043	2.596 ± 0.025	0.130 ± 0.028	976 ± 195	
BH 205	6.780 ± 0.064	1.616 ± 0.031	1.445 ± 0.038	0.148 ± 0.045	1643 ± 328	
BH 23	7.449 ± 0.423	0.432 ± 0.001	0.141 ± 0.425	0.013 ± 0.034	181 ± 36	
BH 87	7.389 ± 0.193	2.041 ± 0.084	1.942 ± 0.046	0.027 ± 0.054	909 ± 181	
BH 90	7.696 ± 0.292	2.384 ± 0.082	1.979 ± 0.097	0.010 ± 0.056	594 ± 118	
BH 92	7.449 ± 0.195	2.301 ± 0.050	1.897 ± 0.060	0.009 ± 0.036	215 ± 43	
Basel 11a	8.036 ± 0.112	1.317 ± 0.027	0.582 ± 0.047	0.126 ± 0.043	242 ± 48	
Basel 11b	8.456 ± 0.045	1.660 ± 0.028	1.918 ± 0.054	0.093 ± 0.049	412 ± 82	
Basel 17	7.913 ± 0.051	2.118 ± 0.087	0.781 ± 0.033	0.016 ± 0.064	798 ± 159	
Basel 18	7.381 ± 0.046	1.722 ± 0.045	1.154 ± 0.047	0.094 ± 0.052	362 ± 72	
Berkeley 1	8.179 ± 0.475	3.541 ± 0.152	2.050 ± 0.083	0.141 ± 0.045	617 ± 123	
Berkeley 10	8.895 ± 0.020	2.093 ± 0.053	2.649 ± 0.070	0.116 ± 0.055	882 ± 176	
Berkeley 11	7.794 ± 0.311	2.436 ± 0.147	2.750 ± 0.040	0.150 ± 0.025	514 ± 102	
Berkeley 15	7.468 ± 0.288	2.140 ± 0.118	2.856 ± 0.071	0.138 ± 0.029	544 ± 108	
Berkeley 28	8.525 ± 0.084	3.585 ± 0.239	2.122 ± 0.075	0.257 ± 0.053	356 ± 71	
Berkeley 30	8.642 ± 0.029	4.091 ± 0.139	1.596 ± 0.027	0.199 ± 0.040	909 ± 181	
Berkeley 37	8.996 ± 0.018	4.396 ± 0.119	0.288 ± 0.024	0.222 ± 0.034	598 ± 119	
Berkeley 4	7.109 ± 0.049	2.698 ± 0.162	2.331 ± 0.051	0.134 ± 0.044	645 ± 129	
Berkeley 47	7.131 ± 0.212	2.182 ± 0.126	3.931 ± 0.047	0.175 ± 0.155	624 ± 124	
Berkeley 6	7.562 ± 0.318	2.448 ± 0.111	2.447 ± 0.063	0.114 ± 0.029	845 ± 169	
Berkeley 60	8.583 ± 0.084	3.060 ± 0.106	2.647 ± 0.039	0.179 ± 0.020	493 ± 98	

Table A1 continued from previous page

Name	log(age)	Dist. (kpc)	Av. (mag.)	FeH	$M_{Tint}(m_{\odot})$	$M_{Tdet}(m_{\odot})$
Berkeley 61	7.926 ± 0.307	2.718 ± 0.085	2.540 ± 0.031	0.115 ± 0.017	364 ± 72	
Berkeley 62	7.274 ± 0.038	2.629 ± 0.078	2.502 ± 0.025	0.127 ± 0.042	1895 ± 379	
Berkeley 69	8.987 ± 0.087	2.857 ± 0.375	2.102 ± 0.116	0.212 ± 0.110	508 ± 101	
Berkeley 7	7.576 ± 0.040	2.433 ± 0.057	2.204 ± 0.033	0.058 ± 0.039	472 ± 94	
Berkeley 77	8.884 ± 0.039	3.753 ± 0.113	0.565 ± 0.050	0.175 ± 0.050	306 ± 61	
Berkeley 8	9.527 ± 0.074	3.013 ± 0.101	2.209 ± 0.100	0.175 ± 0.083	1073 ± 214	
Berkeley 81	8.898 ± 0.058	3.096 ± 0.188	3.150 ± 0.067	0.139 ± 0.035	1972 ± 394	
Berkeley 86	6.869 ± 0.082	1.637 ± 0.065	2.689 ± 0.033	0.051 ± 0.063	585 ± 117	
Berkeley 87	6.915 ± 0.050	1.665 ± 0.051	3.971 ± 0.068	0.051 ± 0.070	1779 ± 355	
Berkeley 94	7.110 ± 0.103	3.742 ± 0.284	1.982 ± 0.049	0.117 ± 0.077	572 ± 114	
Berkeley 96	7.183 ± 0.250	3.327 ± 0.376	1.878 ± 0.065	0.087 ± 0.066	424 ± 84	
Berkeley 97	7.176 ± 0.168	2.601 ± 0.124	2.614 ± 0.042	0.095 ± 0.026	514 ± 102	
Bica 2	6.673 ± 0.045	1.588 ± 0.039	4.486 ± 0.190	0.059 ± 0.094	2150 ± 430	
Biurakan 2	6.907 ± 0.029	1.727 ± 0.047	1.420 ± 0.033	0.027 ± 0.061	627 ± 125	
Blanco 1	8.000 ± 0.001	0.234 ± 0.001	0.010 ± 0.001	0.024 ± 0.001	338 ± 67	
Bochum 3	8.402 ± 0.266	2.165 ± 0.038	0.735 ± 0.078	0.099 ± 0.033	300 ± 60	
Bochum 4	8.244 ± 0.224	1.263 ± 0.021	0.751 ± 0.064	0.080 ± 0.049	93 ± 18	
COINGaia 1	8.296 ± 0.131	0.631 ± 0.004	1.671 ± 0.122	0.004 ± 0.097	266 ± 53	
COINGaia 10	8.168 ± 0.231	0.994 ± 0.017	1.514 ± 0.172	0.082 ± 0.073	200 ± 40	
COINGaia 11	8.753 ± 0.078	0.638 ± 0.005	1.876 ± 0.053	0.001 ± 0.053	332 ± 66	336 ± 67
COINGaia 12	8.767 ± 0.041	0.923 ± 0.007	0.516 ± 0.069	0.081 ± 0.039	229 ± 45	
COINGaia 13	8.215 ± 0.134	0.500 ± 0.001	0.393 ± 0.065	0.092 ± 0.041	378 ± 75	367 ± 73
COINGaia 15	7.986 ± 0.090	1.139 ± 0.017	1.628 ± 0.055	0.012 ± 0.040	402 ± 80	
COINGaia 17	8.125 ± 0.194	1.057 ± 0.012	1.438 ± 0.060	0.142 ± 0.040	264 ± 52	
COINGaia 18	8.275 ± 0.101	0.987 ± 0.011	1.147 ± 0.080	0.093 ± 0.045	251 ± 50	
COINGaia 19	8.506 ± 0.229	1.195 ± 0.016	0.956 ± 0.073	0.037 ± 0.050	261 ± 52	
COINGaia 20	8.254 ± 0.091	1.024 ± 0.007	1.081 ± 0.081	0.128 ± 0.051	220 ± 44	
COINGaia 21	7.238 ± 0.048	1.340 ± 0.035	1.502 ± 0.038	0.029 ± 0.053	199 ± 39	
COINGaia 22	8.322 ± 0.104	1.767 ± 0.042	1.284 ± 0.052	0.067 ± 0.065	297 ± 59	
COINGaia 23	8.329 ± 0.239	0.910 ± 0.003	0.737 ± 0.057	0.068 ± 0.031	245 ± 49	
COINGaia 24	8.252 ± 0.154	0.953 ± 0.012	1.107 ± 0.044	0.082 ± 0.029	185 ± 37	
COINGaia 25	8.791 ± 0.049	0.787 ± 0.005	0.660 ± 0.083	0.046 ± 0.047	311 ± 62	
COINGaia 26	8.148 ± 0.089	1.309 ± 0.014	1.746 ± 0.026	0.025 ± 0.041	352 ± 70	
COINGaia 27	8.618 ± 0.219	1.057 ± 0.019	1.758 ± 0.128	0.154 ± 0.072	265 ± 53	
COINGaia 28	7.953 ± 0.126	1.490 ± 0.030	1.071 ± 0.053	0.105 ± 0.019	388 ± 77	
COINGaia 3	8.022 ± 0.205	1.151 ± 0.030	1.970 ± 0.126	0.251 ± 0.124	350 ± 70	
COINGaia 30	8.254 ± 0.095	0.712 ± 0.004	1.683 ± 0.168	0.072 ± 0.076	211 ± 42	
COINGaia 32	8.211 ± 0.181	1.209 ± 0.018	1.674 ± 0.080	0.121 ± 0.104	114 ± 22	
COINGaia 34	7.877 ± 0.618	0.969 ± 0.059	1.938 ± 0.207	0.029 ± 0.118	79 ± 15	
COINGaia 35	7.745 ± 0.513	2.423 ± 0.080	2.826 ± 0.073	0.099 ± 0.046	454 ± 90	
COINGaia 37	8.037 ± 0.062	0.966 ± 0.012	1.962 ± 0.053	0.046 ± 0.064	150 ± 30	
COINGaia 7	8.031 ± 0.069	1.349 ± 0.033	1.718 ± 0.126	0.002 ± 0.067	254 ± 50	
COINGaia 9	8.274 ± 0.195	0.848 ± 0.007	1.222 ± 0.053	0.001 ± 0.042	162 ± 32	
Collinder 115	8.149 ± 0.109	1.852 ± 0.060	1.153 ± 0.056	0.088 ± 0.055	824 ± 164	
Collinder 140	7.620 ± 0.042	0.378 ± 0.010	0.194 ± 0.055	0.005 ± 0.028	308 ± 61	
Collinder 185	8.036 ± 0.061	1.442 ± 0.026	0.757 ± 0.056	0.031 ± 0.052	245 ± 49	
Collinder 205	6.788 ± 0.050	1.650 ± 0.057	2.561 ± 0.094	0.024 ± 0.070	355 ± 71	
Collinder 258	8.168 ± 0.028	1.210 ± 0.009	0.793 ± 0.068	0.039 ± 0.030	405 ± 81	
Collinder 269	8.585 ± 0.057	1.617 ± 0.024	0.998 ± 0.046	0.013 ± 0.070	477 ± 95	
Collinder 272	7.470 ± 0.044	2.038 ± 0.028	1.540 ± 0.044	0.130 ± 0.038	1316 ± 263	
Collinder 277	8.942 ± 0.031	1.568 ± 0.027	0.952 ± 0.063	0.026 ± 0.042	874 ± 174	
Collinder 292	7.941 ± 0.158	1.747 ± 0.023	1.574 ± 0.046	0.185 ± 0.051	828 ± 165	
Collinder 307	8.151 ± 0.248	1.704 ± 0.033	2.588 ± 0.015	0.171 ± 0.025	713 ± 142	
Collinder 338	8.300 ± 0.112	0.642 ± 0.001	0.713 ± 0.063	0.066 ± 0.055	144 ± 28	
Collinder 394	8.081 ± 0.091	0.705 ± 0.002	0.888 ± 0.049	0.055 ± 0.049	545 ± 109	560 ± 112
Collinder 419	6.693 ± 0.049	0.989 ± 0.012	1.236 ± 0.079	0.044 ± 0.080	155 ± 31	
Collinder 421	7.853 ± 0.341	1.148 ± 0.018	2.445 ± 0.060	0.051 ± 0.075	626 ± 125	
Collinder 74	9.222 ± 0.185	2.261 ± 0.164	1.470 ± 0.229	0.100 ± 0.052	662 ± 132	
Collinder 95	6.856 ± 0.106	0.649 ± 0.002	0.911 ± 0.581	0.111 ± 0.058	379 ± 75	
Czernik 1	7.227 ± 0.173	2.693 ± 0.062	2.394 ± 0.016	0.079 ± 0.044	201 ± 40	

Table A1 continued from previous page

Name	log(age)	Dist. (kpc)	Av. (mag.)	FeH	$M_{Tint}(m_{\odot})$	$M_{Tdet}(m_{\odot})$
Czernik 13	7.978 ± 0.168	2.820 ± 0.041	2.201 ± 0.033	0.163 ± 0.027	850 ± 170	
Czernik 16	8.403 ± 0.072	2.291 ± 0.061	2.941 ± 0.034	0.111 ± 0.050	452 ± 90	
Czernik 19	8.176 ± 0.101	2.117 ± 0.062	2.153 ± 0.026	0.133 ± 0.035	623 ± 124	
Czernik 2	8.545 ± 0.184	1.759 ± 0.057	1.791 ± 0.090	0.037 ± 0.067	398 ± 79	
Czernik 23	8.481 ± 0.031	3.226 ± 0.085	1.794 ± 0.024	0.192 ± 0.029	565 ± 113	
Czernik 27	9.103 ± 0.026	4.062 ± 0.127	0.387 ± 0.042	0.162 ± 0.036	595 ± 119	
Czernik 31	7.471 ± 0.353	2.783 ± 0.065	1.718 ± 0.036	0.150 ± 0.035	576 ± 115	
Czernik 43	7.939 ± 0.344	2.276 ± 0.062	2.054 ± 0.071	0.094 ± 0.072	502 ± 100	
Czernik 5	8.350 ± 0.169	3.207 ± 0.111	3.177 ± 0.050	0.174 ± 0.037	919 ± 183	
Czernik 6	7.363 ± 0.514	2.430 ± 0.242	1.576 ± 0.105	0.099 ± 0.129	238 ± 47	
Czernik 8	7.732 ± 0.185	2.534 ± 0.143	2.993 ± 0.073	0.112 ± 0.067	438 ± 87	
Czernik 9	8.540 ± 0.313	2.512 ± 0.124	3.278 ± 0.087	0.146 ± 0.056	489 ± 97	
DBSB 7	7.387 ± 0.032	2.153 ± 0.100	2.063 ± 0.103	0.098 ± 0.055	1235 ± 247	
Dias 5	6.715 ± 0.153	1.264 ± 0.018	1.537 ± 0.528	0.064 ± 0.056	517 ± 103	
Dolidze 3	6.999 ± 0.072	1.894 ± 0.037	2.266 ± 0.032	0.009 ± 0.091	436 ± 87	
Dolidze 5	7.348 ± 0.255	1.984 ± 0.079	2.669 ± 0.047	0.074 ± 0.074	964 ± 192	
ESO 130 06	8.237 ± 0.181	0.795 ± 0.002	0.514 ± 0.087	0.014 ± 0.074	164 ± 32	
ESO 130 08	8.179 ± 0.141	1.295 ± 0.008	1.240 ± 0.044	0.018 ± 0.031	460 ± 92	
ESO 130 13	7.722 ± 0.139	2.202 ± 0.058	1.619 ± 0.018	0.068 ± 0.067	607 ± 121	
ESO 166 04	8.275 ± 0.115	1.074 ± 0.016	0.690 ± 0.074	0.120 ± 0.076	107 ± 21	
ESO 332 13	6.796 ± 0.059	1.562 ± 0.046	1.420 ± 0.042	0.152 ± 0.071	549 ± 109	
ESO 368 11	8.683 ± 0.276	1.991 ± 0.056	1.769 ± 0.111	0.006 ± 0.029	511 ± 102	
FSR 0198	6.860 ± 0.085	1.843 ± 0.080	2.901 ± 0.172	0.103 ± 0.135	545 ± 109	
FSR 0224	6.722 ± 0.049	1.653 ± 0.037	3.284 ± 0.069	0.040 ± 0.091	177 ± 35	
FSR 0236	6.904 ± 0.081	1.551 ± 0.052	3.813 ± 0.154	0.134 ± 0.072	659 ± 131	
FSR 0241	9.080 ± 0.022	2.060 ± 0.071	1.320 ± 0.050	0.031 ± 0.035	551 ± 110	
FSR 0278	9.403 ± 0.034	1.665 ± 0.024	0.857 ± 0.073	0.017 ± 0.029	542 ± 108	
FSR 0342	8.981 ± 0.062	2.468 ± 0.142	1.666 ± 0.083	0.074 ± 0.060	1503 ± 300	
FSR 0357	7.430 ± 0.265	4.150 ± 0.174	1.752 ± 0.051	0.140 ± 0.039	375 ± 75	
FSR 0384	8.520 ± 0.116	1.847 ± 0.024	1.272 ± 0.054	0.002 ± 0.023	136 ± 27	
FSR 0385	8.789 ± 0.059	2.004 ± 0.091	2.603 ± 0.035	0.028 ± 0.083	304 ± 60	
FSR 0398	7.244 ± 0.082	0.913 ± 0.014	2.071 ± 0.035	0.048 ± 0.127	155 ± 31	
FSR 0430	8.243 ± 0.215	2.460 ± 0.144	3.027 ± 0.056	0.077 ± 0.047	467 ± 93	
FSR 0441	7.779 ± 0.367	3.093 ± 0.150	2.397 ± 0.059	0.094 ± 0.069	379 ± 75	
FSR 0448	8.869 ± 0.269	2.687 ± 0.122	3.102 ± 0.101	0.071 ± 0.041	519 ± 103	
FSR 0496	8.868 ± 0.082	1.377 ± 0.043	3.066 ± 0.087	0.020 ± 0.101	661 ± 132	
FSR 0498	7.562 ± 0.138	2.459 ± 0.080	1.448 ± 0.047	0.034 ± 0.038	329 ± 65	
FSR 0537	7.661 ± 0.057	2.838 ± 0.067	1.754 ± 0.039	0.118 ± 0.022	335 ± 67	
FSR 0551	7.035 ± 0.019	0.892 ± 0.014	1.688 ± 0.056	0.061 ± 0.017	95 ± 19	
FSR 0553	8.885 ± 0.299	2.350 ± 0.185	2.014 ± 0.072	0.063 ± 0.104	122 ± 24	
FSR 0591	7.239 ± 0.093	2.354 ± 0.125	2.201 ± 0.079	0.115 ± 0.059	403 ± 80	
FSR 0667	8.615 ± 0.087	1.097 ± 0.015	1.685 ± 0.086	0.111 ± 0.065	115 ± 23	
FSR 0716	9.087 ± 0.036	3.361 ± 0.159	1.154 ± 0.071	0.262 ± 0.023	513 ± 102	
FSR 0728	8.059 ± 0.189	1.535 ± 0.033	2.137 ± 0.099	0.040 ± 0.033	321 ± 64	
FSR 0735	8.670 ± 0.450	2.568 ± 0.109	1.638 ± 0.133	0.175 ± 0.034	392 ± 78	
FSR 0761	8.746 ± 0.155	2.442 ± 0.122	1.420 ± 0.247	0.119 ± 0.119	188 ± 37	
FSR 0771	8.498 ± 0.023	1.462 ± 0.044	2.179 ± 0.072	0.016 ± 0.067	222 ± 44	
FSR 0811	8.890 ± 0.068	2.470 ± 0.069	0.904 ± 0.119	0.131 ± 0.031	239 ± 47	
FSR 0850	8.576 ± 0.217	1.889 ± 0.101	1.714 ± 0.105	0.099 ± 0.041	513 ± 102	
FSR 0883	8.283 ± 0.320	2.446 ± 0.084	2.123 ± 0.141	0.111 ± 0.059	301 ± 60	
FSR 0893	8.588 ± 0.070	1.957 ± 0.105	2.918 ± 0.106	0.125 ± 0.047	973 ± 194	
FSR 0904	7.176 ± 0.030	2.045 ± 0.042	2.197 ± 0.035	0.096 ± 0.034	900 ± 180	
FSR 0905	8.778 ± 0.060	1.410 ± 0.041	0.526 ± 0.071	0.086 ± 0.056	145 ± 29	
FSR 0935	8.796 ± 0.082	2.262 ± 0.107	1.335 ± 0.098	0.117 ± 0.045	317 ± 63	
FSR 0948	8.651 ± 0.102	3.630 ± 0.146	1.735 ± 0.157	0.205 ± 0.072	351 ± 70	
FSR 0951	8.792 ± 0.262	1.585 ± 0.040	1.210 ± 0.091	0.110 ± 0.025	916 ± 183	
FSR 0968	7.653 ± 0.122	2.245 ± 0.049	1.543 ± 0.038	0.157 ± 0.042	214 ± 42	
FSR 0974	7.334 ± 0.559	2.612 ± 0.245	1.828 ± 0.172	0.175 ± 0.033	630 ± 126	
FSR 0977	8.930 ± 0.198	1.781 ± 0.117	1.595 ± 0.198	0.147 ± 0.060	200 ± 40	
FSR 0985	8.592 ± 0.254	1.950 ± 0.028	1.461 ± 0.080	0.122 ± 0.019	245 ± 49	

Table A1 continued from previous page

Name	log(age)	Dist. (kpc)	Av. (mag.)	FeH	$M_{Tint}(m_{\odot})$	$M_{Tdet}(m_{\odot})$
FSR 1085	8.183 ± 0.138	1.526 ± 0.025	0.867 ± 0.058	0.147 ± 0.031	208 ± 41	
FSR 1144	8.255 ± 0.182	1.786 ± 0.033	0.880 ± 0.047	0.095 ± 0.027	308 ± 61	
FSR 1150	8.798 ± 0.107	3.091 ± 0.159	1.627 ± 0.063	0.114 ± 0.080	368 ± 73	
FSR 1163	8.991 ± 0.049	2.263 ± 0.088	1.617 ± 0.091	0.115 ± 0.029	613 ± 122	
FSR 1180	8.713 ± 0.236	2.552 ± 0.069	1.595 ± 0.096	0.115 ± 0.016	758 ± 151	
FSR 1211	9.105 ± 0.723	3.074 ± 0.486	0.033 ± 0.003	0.027 ± 0.188	381 ± 76	
FSR 1252	8.998 ± 0.034	2.884 ± 0.131	1.159 ± 0.054	0.165 ± 0.056	554 ± 110	
FSR 1253	8.492 ± 0.102	3.644 ± 0.179	2.192 ± 0.067	0.183 ± 0.060	968 ± 193	
FSR 1284	8.882 ± 0.051	2.316 ± 0.068	1.053 ± 0.082	0.045 ± 0.069	195 ± 39	
FSR 1342	7.142 ± 0.066	3.363 ± 0.230	2.697 ± 0.099	0.148 ± 0.040	1021 ± 204	
FSR 1360	8.032 ± 0.109	2.244 ± 0.058	1.552 ± 0.036	0.044 ± 0.031	409 ± 81	
FSR 1361	8.740 ± 0.054	2.190 ± 0.110	2.051 ± 0.115	0.093 ± 0.054	1067 ± 213	
FSR 1363	7.946 ± 0.190	3.237 ± 0.084	1.318 ± 0.061	0.105 ± 0.053	278 ± 55	
FSR 1399	8.771 ± 0.207	2.556 ± 0.315	3.125 ± 0.100	0.017 ± 0.074	351 ± 70	
FSR 1443	8.623 ± 0.423	3.003 ± 0.286	1.805 ± 0.262	0.120 ± 0.059	192 ± 38	
FSR 1484	8.418 ± 0.206	2.074 ± 0.075	2.827 ± 0.096	0.052 ± 0.040	263 ± 52	
FSR 1723	8.119 ± 0.068	1.484 ± 0.029	1.583 ± 0.032	0.075 ± 0.021	412 ± 82	
Gulliver 1	9.122 ± 0.038	2.585 ± 0.077	0.911 ± 0.077	0.033 ± 0.049	885 ± 177	
Gulliver 11	8.341 ± 0.296	0.898 ± 0.005	1.349 ± 0.066	0.001 ± 0.065	106 ± 21	
Gulliver 12	8.221 ± 0.168	1.701 ± 0.045	1.006 ± 0.081	0.012 ± 0.036	142 ± 28	
Gulliver 13	8.815 ± 0.310	1.472 ± 0.024	1.579 ± 0.101	0.115 ± 0.068	351 ± 70	
Gulliver 14	8.672 ± 0.079	1.187 ± 0.068	1.874 ± 0.124	0.201 ± 0.061	170 ± 34	
Gulliver 17	8.019 ± 0.083	1.664 ± 0.027	1.255 ± 0.033	0.137 ± 0.047	511 ± 102	
Gulliver 18	8.063 ± 0.015	1.515 ± 0.022	2.074 ± 0.061	0.106 ± 0.054	888 ± 177	
Gulliver 20	8.853 ± 0.085	0.415 ± 0.008	0.297 ± 0.041	0.025 ± 0.036	136 ± 27	
Gulliver 21	8.177 ± 0.177	0.638 ± 0.001	0.046 ± 0.016	0.111 ± 0.156	281 ± 56	
Gulliver 24	8.266 ± 0.191	1.415 ± 0.016	1.515 ± 0.078	0.005 ± 0.056	218 ± 43	
Gulliver 25	8.472 ± 0.204	1.292 ± 0.017	1.072 ± 0.083	0.110 ± 0.055	258 ± 51	
Gulliver 26	8.670 ± 0.187	2.444 ± 0.155	2.116 ± 0.070	0.123 ± 0.101	357 ± 71	
Gulliver 27	8.200 ± 0.196	2.537 ± 0.094	1.794 ± 0.090	0.008 ± 0.038	555 ± 111	
Gulliver 28	9.001 ± 0.469	0.502 ± 0.127	1.297 ± 0.463	0.229 ± 0.051	180 ± 36	
Gulliver 31	8.249 ± 0.115	2.129 ± 0.059	1.556 ± 0.035	0.112 ± 0.060	371 ± 74	
Gulliver 32	8.737 ± 0.536	1.627 ± 0.068	1.553 ± 0.280	0.164 ± 0.084	181 ± 36	
Gulliver 35	8.091 ± 0.223	2.025 ± 0.051	1.342 ± 0.064	0.058 ± 0.061	281 ± 56	
Gulliver 36	8.849 ± 0.141	1.278 ± 0.018	0.969 ± 0.129	0.080 ± 0.063	260 ± 52	
Gulliver 37	8.261 ± 0.161	1.479 ± 0.032	1.893 ± 0.062	0.036 ± 0.106	306 ± 61	
Gulliver 39	8.852 ± 0.177	2.465 ± 0.119	1.769 ± 0.123	0.048 ± 0.060	373 ± 74	
Gulliver 40	7.901 ± 0.204	1.524 ± 0.021	0.671 ± 0.102	0.151 ± 0.071	131 ± 26	
Gulliver 44	8.788 ± 0.096	1.178 ± 0.017	1.471 ± 0.096	0.031 ± 0.070	379 ± 75	
Gulliver 47	8.621 ± 0.039	1.847 ± 0.045	0.448 ± 0.051	0.116 ± 0.032	466 ± 93	
Gulliver 5	7.083 ± 0.051	2.054 ± 0.094	2.117 ± 0.068	0.075 ± 0.062	394 ± 78	
Gulliver 50	8.023 ± 0.151	1.657 ± 0.029	1.081 ± 0.033	0.054 ± 0.051	421 ± 84	
Gulliver 56	8.520 ± 0.140	1.956 ± 0.055	0.899 ± 0.086	0.084 ± 0.033	269 ± 53	
Gulliver 59	8.019 ± 0.349	1.944 ± 0.094	1.550 ± 0.145	0.079 ± 0.041	411 ± 82	
Gulliver 6	7.124 ± 0.014	0.408 ± 0.001	0.485 ± 0.088	0.034 ± 0.024	365 ± 73	
Gulliver 60	7.992 ± 0.179	1.047 ± 0.012	1.360 ± 0.066	0.184 ± 0.059	347 ± 69	
Gulliver 8	7.437 ± 0.076	1.037 ± 0.020	1.049 ± 0.077	0.022 ± 0.085	156 ± 31	
Haffner 13	7.541 ± 0.026	0.551 ± 0.001	0.247 ± 0.029	0.057 ± 0.032	393 ± 78	
Haffner 16	8.324 ± 0.331	2.786 ± 0.072	0.388 ± 0.033	0.058 ± 0.054	511 ± 102	
Haffner 20	8.271 ± 0.275	3.542 ± 0.107	2.224 ± 0.057	0.174 ± 0.043	377 ± 75	
Haffner 21	8.804 ± 0.055	2.683 ± 0.072	0.366 ± 0.028	0.020 ± 0.047	270 ± 54	
Haffner 23	8.695 ± 0.097	1.965 ± 0.051	0.839 ± 0.081	0.021 ± 0.038	561 ± 112	
Haffner 26	8.820 ± 0.036	2.635 ± 0.058	0.620 ± 0.057	0.055 ± 0.055	602 ± 120	
Haffner 3	8.722 ± 0.098	2.332 ± 0.041	1.329 ± 0.075	0.142 ± 0.028	275 ± 55	
Haffner 4	8.865 ± 0.428	4.203 ± 0.258	1.489 ± 0.184	0.237 ± 0.038	1119 ± 223	
Haffner 6	8.633 ± 0.120	4.106 ± 0.188	2.079 ± 0.079	0.219 ± 0.026	1745 ± 349	
Haffner 7	8.838 ± 0.035	4.016 ± 0.119	0.811 ± 0.052	0.106 ± 0.063	422 ± 84	
Haffner 8	8.532 ± 0.164	2.496 ± 0.049	1.290 ± 0.061	0.116 ± 0.060	633 ± 126	
Haffner 9	7.970 ± 0.267	2.647 ± 0.105	2.215 ± 0.056	0.145 ± 0.029	582 ± 116	
Harvard 10	8.267 ± 0.099	0.671 ± 0.004	0.586 ± 0.049	0.024 ± 0.029	425 ± 85	422 ± 84

Table A1 continued from previous page

Name	log(age)	Dist. (kpc)	Av. (mag.)	FeH	$M_{Tint}(m_{\odot})$	$M_{Tdet}(m_{\odot})$
Harvard 20	8.027 ± 0.099	2.234 ± 0.071	0.936 ± 0.059	0.002 ± 0.063	483 ± 96	
Hogg 16	7.415 ± 0.056	1.996 ± 0.041	1.486 ± 0.041	0.119 ± 0.051	232 ± 46	
Hogg 22	6.945 ± 0.071	2.416 ± 0.102	2.169 ± 0.018	0.064 ± 0.073	444 ± 88	
Hogg 4	8.999 ± 0.038	3.484 ± 0.164	1.917 ± 0.065	0.046 ± 0.065	2165 ± 433	
IC 1369	8.490 ± 0.229	2.870 ± 0.099	2.563 ± 0.058	0.009 ± 0.030	1262 ± 252	
IC 1434	8.118 ± 0.266	3.016 ± 0.128	1.454 ± 0.045	0.047 ± 0.066	1432 ± 286	
IC 1442	7.465 ± 0.087	2.808 ± 0.112	1.547 ± 0.050	0.082 ± 0.052	1473 ± 294	
IC 1590	6.871 ± 0.139	2.532 ± 0.188	1.315 ± 0.088	0.128 ± 0.073	651 ± 130	
IC 2157	7.738 ± 0.282	1.877 ± 0.049	1.587 ± 0.048	0.037 ± 0.055	189 ± 37	
IC 2391	7.761 ± 0.021	0.149 ± 0.001	0.088 ± 0.032	0.124 ± 0.040	215 ± 43	
IC 2395	7.122 ± 0.023	0.693 ± 0.004	0.474 ± 0.044	0.034 ± 0.039	484 ± 96	482 ± 96
IC 2488	8.184 ± 0.036	1.287 ± 0.012	0.979 ± 0.024	0.019 ± 0.025	1190 ± 238	1234 ± 246
IC 2581	7.135 ± 0.079	2.421 ± 0.114	1.435 ± 0.022	0.041 ± 0.071	834 ± 166	
IC 2602	7.700 ± 0.043	0.149 ± 0.001	0.104 ± 0.064	0.121 ± 0.060	264 ± 52	
IC 2948	6.814 ± 0.063	2.242 ± 0.081	1.351 ± 0.023	0.007 ± 0.084	1025 ± 205	
IC 361	9.014 ± 0.034	3.385 ± 0.113	2.374 ± 0.044	0.229 ± 0.041	2459 ± 491	
IC 4665	8.309 ± 0.270	0.310 ± 0.013	0.510 ± 0.148	0.112 ± 0.066	308 ± 61	
IC 4996	7.027 ± 0.023	1.912 ± 0.080	1.863 ± 0.049	0.076 ± 0.065	500 ± 100	
Juchert 20	8.005 ± 0.619	2.603 ± 0.078	2.410 ± 0.163	0.188 ± 0.047	707 ± 141	
Kharchenko 1	8.671 ± 0.077	2.407 ± 0.093	1.549 ± 0.114	0.186 ± 0.041	348 ± 69	
King 12	7.259 ± 0.097	2.491 ± 0.099	1.837 ± 0.053	0.099 ± 0.059	300 ± 60	
King 13	8.760 ± 0.045	3.230 ± 0.107	2.194 ± 0.051	0.155 ± 0.030	1577 ± 315	
King 14	7.470 ± 0.110	2.232 ± 0.086	1.681 ± 0.040	0.019 ± 0.042	870 ± 174	
King 15	8.006 ± 0.537	2.730 ± 0.079	2.063 ± 0.082	0.109 ± 0.039	452 ± 90	
King 16	7.378 ± 0.322	2.506 ± 0.046	2.528 ± 0.049	0.063 ± 0.055	633 ± 126	
King 17	7.559 ± 0.450	3.318 ± 0.075	1.876 ± 0.096	0.263 ± 0.034	281 ± 56	
King 18	8.404 ± 0.049	2.501 ± 0.079	2.096 ± 0.063	0.090 ± 0.027	718 ± 143	
King 19	8.775 ± 0.042	2.487 ± 0.081	2.438 ± 0.062	0.005 ± 0.046	676 ± 135	
King 20	7.623 ± 0.128	1.709 ± 0.030	2.589 ± 0.037	0.113 ± 0.078	471 ± 94	
King 21	7.196 ± 0.107	2.811 ± 0.147	2.597 ± 0.034	0.114 ± 0.050	1078 ± 215	
King 4	7.923 ± 0.347	2.203 ± 0.062	2.535 ± 0.051	0.112 ± 0.044	888 ± 177	
King 5	8.961 ± 0.038	2.186 ± 0.114	2.586 ± 0.046	0.129 ± 0.030	1275 ± 255	
King 6	8.072 ± 0.193	0.702 ± 0.001	1.909 ± 0.062	0.041 ± 0.060	497 ± 99	
Koposov 10	8.279 ± 0.348	2.377 ± 0.120	2.505 ± 0.099	0.192 ± 0.036	457 ± 91	
Koposov 12	8.651 ± 0.122	2.105 ± 0.066	1.852 ± 0.062	0.101 ± 0.030	851 ± 170	
Koposov 36	7.623 ± 0.417	1.640 ± 0.060	2.577 ± 0.236	0.112 ± 0.062	537 ± 107	
Koposov 43	9.040 ± 0.042	4.658 ± 0.284	2.047 ± 0.097	0.307 ± 0.079	948 ± 189	
Kronberger 4	8.908 ± 0.072	6.866 ± 0.742	2.575 ± 0.103	0.072 ± 0.086	750 ± 150	
LP 0201	7.313 ± 0.114	3.408 ± 0.196	2.320 ± 0.039	0.142 ± 0.051	656 ± 131	
LP 0665	9.056 ± 0.054	3.331 ± 0.163	1.333 ± 0.100	0.068 ± 0.058	573 ± 114	
LP 0733	7.523 ± 0.031	2.613 ± 0.082	1.108 ± 0.021	0.149 ± 0.039	936 ± 187	
LP 0782	8.256 ± 0.177	3.152 ± 0.111	1.882 ± 0.111	0.001 ± 0.037	346 ± 69	
LP 1406	8.646 ± 0.314	2.597 ± 0.155	1.535 ± 0.130	0.172 ± 0.047	270 ± 54	
LP 1540	9.161 ± 0.026	2.454 ± 0.076	0.814 ± 0.064	0.008 ± 0.039	934 ± 186	
LP 1614	7.804 ± 0.337	2.121 ± 0.073	3.276 ± 0.066	0.152 ± 0.036	818 ± 163	
LP 1800	8.277 ± 0.112	1.329 ± 0.030	1.761 ± 0.065	0.038 ± 0.039	1017 ± 203	
LP 1809	8.338 ± 0.292	2.596 ± 0.148	2.857 ± 0.078	0.016 ± 0.055	487 ± 97	
LP 198	8.441 ± 0.275	2.840 ± 0.065	1.177 ± 0.060	0.127 ± 0.038	916 ± 183	
LP 1994	8.824 ± 0.039	1.812 ± 0.040	1.461 ± 0.047	0.040 ± 0.045	638 ± 127	
LP 2000	8.157 ± 0.083	1.313 ± 0.016	1.783 ± 0.036	0.154 ± 0.045	654 ± 130	
LP 2059	7.996 ± 0.076	2.149 ± 0.050	0.762 ± 0.045	0.107 ± 0.038	607 ± 121	
LP 2068	8.270 ± 0.061	1.831 ± 0.033	2.170 ± 0.047	0.130 ± 0.033	850 ± 170	
LP 2094	8.334 ± 0.114	1.614 ± 0.028	0.876 ± 0.038	0.042 ± 0.030	569 ± 113	
LP 2123	8.128 ± 0.057	1.547 ± 0.076	2.127 ± 0.051	0.046 ± 0.088	305 ± 61	
LP 2219	8.031 ± 0.071	1.416 ± 0.018	1.303 ± 0.046	0.043 ± 0.003	1444 ± 288	
LP 2220	8.705 ± 0.063	1.288 ± 0.012	1.057 ± 0.106	0.100 ± 0.057	365 ± 73	
LP 2238	8.712 ± 0.150	1.146 ± 0.012	0.440 ± 0.081	0.105 ± 0.050	288 ± 57	
LP 2253	8.045 ± 0.144	1.384 ± 0.023	1.611 ± 0.106	0.027 ± 0.073	384 ± 76	
LP 2312	8.162 ± 0.216	1.025 ± 0.010	1.753 ± 0.105	0.042 ± 0.097	198 ± 39	
LP 2339	7.948 ± 0.232	1.034 ± 0.008	2.652 ± 0.039	0.156 ± 0.047	244 ± 48	

Table A1 continued from previous page

Name	log(age)	Dist. (kpc)	Av. (mag.)	FeH	$M_{Tint}(m_{\odot})$	$M_{Tdet}(m_{\odot})$
LP 589	8.702 ± 0.043	2.826 ± 0.060	0.268 ± 0.036	0.117 ± 0.033	524 ± 104	
LP 597	8.795 ± 0.306	2.004 ± 0.085	2.942 ± 0.115	0.119 ± 0.053	1099 ± 219	
LP 658	9.013 ± 0.020	1.400 ± 0.020	0.811 ± 0.070	0.103 ± 0.039	420 ± 84	
LP 866	9.521 ± 0.154	2.104 ± 0.171	2.261 ± 0.159	0.099 ± 0.047	1219 ± 243	
LP 930	9.200 ± 0.031	2.276 ± 0.064	1.046 ± 0.080	0.032 ± 0.062	508 ± 101	
Loden 1194	8.373 ± 0.069	0.717 ± 0.004	0.764 ± 0.046	0.027 ± 0.027	140 ± 28	
Loden 372	8.149 ± 0.105	1.665 ± 0.041	1.087 ± 0.060	0.092 ± 0.058	380 ± 76	
Loden 46	8.915 ± 0.062	1.093 ± 0.006	0.483 ± 0.135	0.119 ± 0.063	288 ± 57	
Lynga 2	8.050 ± 0.121	0.918 ± 0.007	1.026 ± 0.031	0.050 ± 0.035	367 ± 73	
Majaess 65	8.054 ± 0.093	0.926 ± 0.007	0.808 ± 0.044	0.048 ± 0.040	98 ± 19	
Mamajek 4	8.772 ± 0.041	0.442 ± 0.010	0.335 ± 0.073	0.006 ± 0.056	506 ± 101	497 ± 99
Markarian 38	7.164 ± 0.161	1.662 ± 0.048	1.061 ± 0.048	0.031 ± 0.071	156 ± 31	
Melotte 22	8.005 ± 0.016	0.135 ± 0.001	0.349 ± 0.036	0.017 ± 0.010	816 ± 163	838 ± 167
Melotte 72	9.097 ± 0.026	2.578 ± 0.089	0.230 ± 0.016	0.066 ± 0.063	709 ± 141	
NGC 1027	8.104 ± 0.129	1.069 ± 0.004	1.486 ± 0.062	0.038 ± 0.047	879 ± 175	
NGC 103	7.996 ± 0.142	2.984 ± 0.064	1.723 ± 0.041	0.123 ± 0.035	841 ± 168	
NGC 1220	7.553 ± 0.224	2.493 ± 0.049	2.477 ± 0.028	0.113 ± 0.027	255 ± 51	
NGC 129	7.963 ± 0.038	1.723 ± 0.026	1.854 ± 0.026	0.002 ± 0.052	1577 ± 315	
NGC 1342	8.605 ± 0.095	0.636 ± 0.003	1.263 ± 0.045	0.005 ± 0.028	925 ± 185	835 ± 167
NGC 146	7.400 ± 0.079	2.598 ± 0.103	1.849 ± 0.030	0.093 ± 0.048	759 ± 151	
NGC 1496	8.544 ± 0.116	1.529 ± 0.033	1.808 ± 0.078	0.091 ± 0.071	199 ± 39	
NGC 1502	6.881 ± 0.065	1.019 ± 0.010	2.236 ± 0.045	0.170 ± 0.093	728 ± 145	
NGC 1513	8.230 ± 0.186	1.352 ± 0.019	2.228 ± 0.045	0.004 ± 0.040	850 ± 170	
NGC 1528	8.540 ± 0.106	0.986 ± 0.008	1.149 ± 0.036	0.007 ± 0.040	925 ± 185	
NGC 1545	8.126 ± 0.238	0.692 ± 0.004	1.237 ± 0.081	0.030 ± 0.044	287 ± 57	
NGC 1582	8.188 ± 0.150	0.941 ± 0.008	1.278 ± 0.025	0.096 ± 0.030	534 ± 106	
NGC 1605	7.799 ± 0.423	2.463 ± 0.102	2.679 ± 0.087	0.151 ± 0.038	610 ± 122	
NGC 1662	8.847 ± 0.083	0.388 ± 0.014	1.159 ± 0.088	0.170 ± 0.055	397 ± 79	391 ± 78
NGC 1664	8.744 ± 0.039	1.279 ± 0.013	0.923 ± 0.054	0.005 ± 0.044	778 ± 155	823 ± 164
NGC 1708	8.296 ± 0.113	0.906 ± 0.010	1.767 ± 0.057	0.175 ± 0.048	390 ± 78	
NGC 1750	8.187 ± 0.149	0.695 ± 0.003	1.236 ± 0.048	0.001 ± 0.025	705 ± 141	
NGC 1758	8.742 ± 0.028	0.850 ± 0.011	1.268 ± 0.065	0.018 ± 0.038	333 ± 66	
NGC 1778	7.989 ± 0.129	1.538 ± 0.021	1.382 ± 0.029	0.069 ± 0.038	535 ± 107	
NGC 1857	8.436 ± 0.045	2.512 ± 0.059	1.670 ± 0.036	0.123 ± 0.029	732 ± 146	
NGC 1883	8.627 ± 0.092	3.802 ± 0.158	1.823 ± 0.057	0.293 ± 0.049	591 ± 118	
NGC 189	8.806 ± 0.098	1.208 ± 0.028	1.831 ± 0.118	0.048 ± 0.116	281 ± 56	
NGC 1901	8.887 ± 0.116	0.416 ± 0.001	0.208 ± 0.089	0.030 ± 0.018	197 ± 39	
NGC 1907	8.815 ± 0.058	1.450 ± 0.027	1.502 ± 0.079	0.115 ± 0.049	677 ± 135	636 ± 127
NGC 1912	8.505 ± 0.043	1.069 ± 0.012	0.998 ± 0.032	0.022 ± 0.025	1462 ± 292	1447 ± 289
NGC 1960	7.451 ± 0.032	1.119 ± 0.011	0.904 ± 0.024	0.026 ± 0.028	629 ± 125	
NGC 2126	9.181 ± 0.021	1.254 ± 0.018	0.806 ± 0.060	0.141 ± 0.050	275 ± 55	
NGC 2129	7.357 ± 0.137	1.815 ± 0.051	2.213 ± 0.063	0.080 ± 0.091	453 ± 90	
NGC 2169	6.899 ± 0.058	0.936 ± 0.016	0.805 ± 0.056	0.179 ± 0.057	234 ± 46	
NGC 2183	6.858 ± 0.108	0.825 ± 0.010	1.657 ± 0.522	0.120 ± 0.043	258 ± 51	
NGC 2184	8.970 ± 0.047	0.562 ± 0.002	0.655 ± 0.072	0.121 ± 0.052	196 ± 39	
NGC 2192	9.149 ± 0.037	3.382 ± 0.132	0.436 ± 0.046	0.164 ± 0.057	765 ± 153	
NGC 2215	8.817 ± 0.051	0.922 ± 0.007	0.794 ± 0.071	0.048 ± 0.052	371 ± 74	
NGC 2225	9.095 ± 0.044	2.889 ± 0.141	1.630 ± 0.056	0.199 ± 0.036	470 ± 94	
NGC 2232	7.451 ± 0.036	0.314 ± 0.006	0.236 ± 0.034	0.035 ± 0.040	227 ± 45	
NGC 2236	8.954 ± 0.024	2.421 ± 0.053	1.674 ± 0.044	0.153 ± 0.043	1331 ± 266	
NGC 225	8.238 ± 0.142	0.668 ± 0.004	0.923 ± 0.078	0.143 ± 0.091	124 ± 24	
NGC 2259	8.499 ± 0.082	2.619 ± 0.074	1.996 ± 0.050	0.160 ± 0.026	406 ± 81	
NGC 2262	8.983 ± 0.061	2.824 ± 0.266	2.294 ± 0.080	0.142 ± 0.039	1004 ± 200	
NGC 2264	6.744 ± 0.076	0.692 ± 0.006	0.328 ± 0.110	0.041 ± 0.046	368 ± 73	
NGC 2266	9.021 ± 0.023	3.114 ± 0.094	0.436 ± 0.061	0.232 ± 0.040	840 ± 168	
NGC 2269	8.397 ± 0.188	2.046 ± 0.070	1.358 ± 0.094	0.105 ± 0.032	306 ± 61	
NGC 2281	8.736 ± 0.043	0.508 ± 0.001	0.341 ± 0.057	0.032 ± 0.037	681 ± 136	
NGC 2286	8.752 ± 0.086	2.042 ± 0.055	1.133 ± 0.121	0.108 ± 0.052	557 ± 111	
NGC 2287	8.296 ± 0.067	0.714 ± 0.004	0.225 ± 0.032	0.078 ± 0.025	1126 ± 225	1185 ± 237
NGC 2301	8.306 ± 0.053	0.835 ± 0.006	0.251 ± 0.012	0.031 ± 0.018	725 ± 145	793 ± 158

Table A1 continued from previous page

Name	log(age)	Dist. (kpc)	Av. (mag.)	FeH	$M_{Tint}(m_{\odot})$	$M_{Tdet}(m_{\odot})$
NGC 2302	8.090 ± 0.072	1.167 ± 0.004	0.734 ± 0.047	0.033 ± 0.018	190 ± 38	
NGC 2311	7.798 ± 0.193	1.910 ± 0.040	1.186 ± 0.054	0.045 ± 0.040	365 ± 73	
NGC 2318	8.709 ± 0.087	1.278 ± 0.023	1.075 ± 0.106	0.013 ± 0.026	561 ± 112	
NGC 2343	8.190 ± 0.150	1.040 ± 0.014	0.674 ± 0.095	0.013 ± 0.058	194 ± 38	
NGC 2354	9.204 ± 0.020	1.262 ± 0.022	0.488 ± 0.052	0.061 ± 0.035	847 ± 169	
NGC 2355	9.094 ± 0.028	1.777 ± 0.020	0.301 ± 0.019	0.004 ± 0.044	705 ± 141	660 ± 132
NGC 2360	9.106 ± 0.029	1.036 ± 0.009	0.396 ± 0.041	0.083 ± 0.027	1327 ± 265	1317 ± 263
NGC 2374	8.575 ± 0.047	1.211 ± 0.012	0.515 ± 0.047	0.029 ± 0.041	257 ± 51	
NGC 2383	8.451 ± 0.067	2.822 ± 0.082	1.087 ± 0.027	0.144 ± 0.037	763 ± 152	
NGC 2384	7.372 ± 0.118	2.270 ± 0.130	0.910 ± 0.040	0.130 ± 0.123	313 ± 62	
NGC 2396	8.202 ± 0.055	1.375 ± 0.027	0.569 ± 0.031	0.129 ± 0.036	670 ± 134	
NGC 2401	7.812 ± 0.277	4.239 ± 0.223	1.285 ± 0.054	0.220 ± 0.032	444 ± 88	
NGC 2414	7.157 ± 0.058	4.173 ± 0.170	1.828 ± 0.013	0.224 ± 0.027	1384 ± 276	
NGC 2421	7.833 ± 0.171	2.368 ± 0.063	1.447 ± 0.038	0.109 ± 0.034	1344 ± 268	
NGC 2423	9.048 ± 0.021	0.901 ± 0.009	0.353 ± 0.042	0.024 ± 0.044	999 ± 199	
NGC 2428	8.888 ± 0.023	1.299 ± 0.013	0.272 ± 0.022	0.030 ± 0.025	461 ± 92	
NGC 2432	8.968 ± 0.043	1.731 ± 0.029	0.772 ± 0.066	0.003 ± 0.062	705 ± 141	
NGC 2439	7.379 ± 0.066	3.330 ± 0.076	1.351 ± 0.020	0.178 ± 0.023	2656 ± 531	
NGC 2448	8.117 ± 0.186	1.070 ± 0.018	0.062 ± 0.013	0.059 ± 0.044	450 ± 90	
NGC 2451A	7.716 ± 0.041	0.192 ± 0.001	0.073 ± 0.037	0.045 ± 0.037	342 ± 68	371 ± 74
NGC 2451B	7.631 ± 0.026	0.354 ± 0.004	0.463 ± 0.053	0.011 ± 0.015	367 ± 73	
NGC 2453	7.457 ± 0.218	3.838 ± 0.089	1.645 ± 0.037	0.151 ± 0.034	656 ± 131	
NGC 2479	9.101 ± 0.025	1.561 ± 0.016	0.069 ± 0.010	0.066 ± 0.041	395 ± 79	327 ± 65
NGC 2482	8.827 ± 0.048	1.208 ± 0.035	0.096 ± 0.022	0.102 ± 0.112	313 ± 62	
NGC 2489	8.565 ± 0.095	1.778 ± 0.055	1.514 ± 0.050	0.051 ± 0.070	1136 ± 227	
NGC 2509	9.146 ± 0.001	2.831 ± 0.001	0.055 ± 0.001	0.426 ± 0.001	1453 ± 290	
NGC 2533	9.001 ± 0.044	2.532 ± 0.100	1.040 ± 0.100	0.032 ± 0.055	632 ± 126	
NGC 2539	8.890 ± 0.019	1.239 ± 0.009	0.135 ± 0.011	0.005 ± 0.023	1152 ± 230	1083 ± 216
NGC 2546	8.244 ± 0.030	0.903 ± 0.005	0.536 ± 0.039	0.023 ± 0.036	558 ± 111	606 ± 121
NGC 2547	7.551 ± 0.095	0.384 ± 0.004	0.352 ± 0.132	0.032 ± 0.076	362 ± 72	
NGC 2548	8.714 ± 0.032	0.747 ± 0.004	0.127 ± 0.016	0.002 ± 0.026	920 ± 184	912 ± 182
NGC 2571	7.419 ± 0.166	1.248 ± 0.023	0.435 ± 0.028	0.038 ± 0.043	345 ± 69	
NGC 2587	8.831 ± 0.037	2.751 ± 0.079	0.223 ± 0.025	0.006 ± 0.050	649 ± 129	
NGC 2645	7.318 ± 0.086	1.707 ± 0.046	1.439 ± 0.028	0.001 ± 0.088	348 ± 69	
NGC 2659	7.543 ± 0.180	1.909 ± 0.031	1.598 ± 0.048	0.003 ± 0.055	404 ± 80	
NGC 2669	8.114 ± 0.073	1.110 ± 0.009	0.866 ± 0.060	0.003 ± 0.034	509 ± 101	
NGC 2670	8.098 ± 0.054	1.394 ± 0.019	1.417 ± 0.040	0.148 ± 0.073	562 ± 112	
NGC 2671	8.617 ± 0.314	1.335 ± 0.022	2.823 ± 0.071	0.020 ± 0.036	943 ± 188	
NGC 2682	9.578 ± 0.021	0.842 ± 0.005	0.164 ± 0.029	0.045 ± 0.041	1843 ± 368	
NGC 2818	9.099 ± 0.031	2.908 ± 0.093	0.535 ± 0.087	0.097 ± 0.070	1100 ± 220	
NGC 2866	8.045 ± 0.132	2.370 ± 0.048	2.052 ± 0.033	0.015 ± 0.035	364 ± 72	
NGC 2910	8.017 ± 0.111	1.220 ± 0.011	0.790 ± 0.059	0.051 ± 0.061	419 ± 83	
NGC 2925	8.320 ± 0.194	0.738 ± 0.005	0.260 ± 0.074	0.008 ± 0.050	219 ± 43	203 ± 40
NGC 2972	8.631 ± 0.078	1.816 ± 0.056	1.575 ± 0.084	0.029 ± 0.032	335 ± 67	
NGC 3033	8.841 ± 0.065	1.689 ± 0.034	1.028 ± 0.079	0.040 ± 0.022	441 ± 88	
NGC 3228	7.721 ± 0.128	0.461 ± 0.014	0.205 ± 0.071	0.001 ± 0.067	228 ± 45	
NGC 3255	8.546 ± 0.135	4.777 ± 0.145	1.305 ± 0.091	0.036 ± 0.030	992 ± 198	
NGC 3293	7.145 ± 0.039	2.283 ± 0.068	0.947 ± 0.017	0.017 ± 0.036	1975 ± 395	
NGC 3496	8.734 ± 0.024	2.158 ± 0.038	1.553 ± 0.045	0.153 ± 0.039	2044 ± 408	
NGC 3590	7.151 ± 0.035	2.259 ± 0.109	1.615 ± 0.032	0.041 ± 0.071	735 ± 147	
NGC 3680	9.302 ± 0.041	1.013 ± 0.009	0.310 ± 0.102	0.137 ± 0.060	366 ± 73	
NGC 381	8.548 ± 0.095	1.119 ± 0.011	1.436 ± 0.047	0.011 ± 0.048	369 ± 73	
NGC 3960	8.975 ± 0.041	2.098 ± 0.078	1.098 ± 0.142	0.021 ± 0.079	1152 ± 230	
NGC 433	7.856 ± 0.070	1.817 ± 0.058	2.242 ± 0.050	0.104 ± 0.052	459 ± 91	
NGC 4337	9.172 ± 0.012	2.367 ± 0.044	1.291 ± 0.037	0.047 ± 0.029	1049 ± 209	
NGC 436	7.924 ± 0.105	2.829 ± 0.059	1.595 ± 0.026	0.088 ± 0.057	829 ± 165	
NGC 4439	7.723 ± 0.055	1.780 ± 0.056	1.234 ± 0.032	0.055 ± 0.070	282 ± 56	
NGC 4463	7.492 ± 0.181	1.684 ± 0.043	1.615 ± 0.062	0.134 ± 0.045	555 ± 111	
NGC 4609	7.878 ± 0.070	1.366 ± 0.019	1.233 ± 0.048	0.097 ± 0.042	943 ± 188	
NGC 4852	8.056 ± 0.060	1.245 ± 0.019	1.448 ± 0.021	0.007 ± 0.062	983 ± 196	

Table A1 continued from previous page

Name	log(age)	Dist. (kpc)	Av. (mag.)	FeH	$M_{Tint}(m_{\odot})$	$M_{Tdet}(m_{\odot})$
NGC 5138	8.023 ± 0.160	1.840 ± 0.044	0.842 ± 0.056	0.125 ± 0.086	448 ± 89	
NGC 5168	8.848 ± 0.051	2.554 ± 0.086	1.947 ± 0.096	0.099 ± 0.049	795 ± 159	
NGC 5269	8.226 ± 0.200	1.850 ± 0.046	1.477 ± 0.060	0.168 ± 0.050	386 ± 77	
NGC 5281	7.802 ± 0.091	1.461 ± 0.023	1.031 ± 0.026	0.028 ± 0.055	423 ± 84	
NGC 5288	8.588 ± 0.347	2.287 ± 0.075	1.705 ± 0.138	0.094 ± 0.055	475 ± 95	
NGC 5316	8.138 ± 0.186	1.395 ± 0.023	1.133 ± 0.062	0.052 ± 0.053	453 ± 90	
NGC 5460	8.249 ± 0.160	0.707 ± 0.003	0.475 ± 0.073	0.052 ± 0.033	379 ± 75	
NGC 559	8.757 ± 0.037	2.353 ± 0.041	2.214 ± 0.036	0.095 ± 0.034	1949 ± 389	
NGC 5593	8.297 ± 0.076	1.002 ± 0.012	0.916 ± 0.065	0.011 ± 0.053	245 ± 49	
NGC 5662	8.074 ± 0.176	0.749 ± 0.004	1.116 ± 0.047	0.021 ± 0.034	658 ± 131	691 ± 138
NGC 5715	8.676 ± 0.104	1.919 ± 0.059	2.118 ± 0.071	0.155 ± 0.033	927 ± 185	
NGC 5749	8.122 ± 0.059	1.071 ± 0.011	1.176 ± 0.044	0.027 ± 0.061	276 ± 55	
NGC 581	7.822 ± 0.184	2.329 ± 0.045	1.407 ± 0.031	0.078 ± 0.058	715 ± 143	
NGC 5999	8.213 ± 0.204	2.294 ± 0.081	1.944 ± 0.045	0.135 ± 0.051	1203 ± 240	
NGC 6025	8.173 ± 0.078	0.753 ± 0.003	0.690 ± 0.031	0.001 ± 0.017	575 ± 115	609 ± 121
NGC 6031	7.705 ± 0.202	1.705 ± 0.030	1.632 ± 0.054	0.137 ± 0.063	527 ± 105	
NGC 6087	8.192 ± 0.083	0.924 ± 0.014	0.704 ± 0.027	0.118 ± 0.077	668 ± 133	678 ± 135
NGC 6134	9.096 ± 0.024	1.078 ± 0.009	1.300 ± 0.037	0.025 ± 0.029	1912 ± 382	1824 ± 364
NGC 6152	8.309 ± 0.098	1.534 ± 0.026	1.283 ± 0.045	0.040 ± 0.027	1228 ± 245	
NGC 6178	7.123 ± 0.068	0.849 ± 0.018	0.868 ± 0.096	0.026 ± 0.085	122 ± 24	
NGC 6192	7.677 ± 0.234	1.553 ± 0.030	2.222 ± 0.059	0.140 ± 0.050	1840 ± 368	
NGC 6204	8.013 ± 0.073	1.129 ± 0.016	1.523 ± 0.024	0.070 ± 0.029	628 ± 125	
NGC 6208	9.269 ± 0.023	1.142 ± 0.009	1.082 ± 0.067	0.228 ± 0.040	1689 ± 337	
NGC 6242	7.833 ± 0.086	1.219 ± 0.016	1.374 ± 0.024	0.126 ± 0.041	1529 ± 305	
NGC 6249	7.346 ± 0.042	1.144 ± 0.012	1.570 ± 0.060	0.076 ± 0.060	297 ± 59	
NGC 6253	9.525 ± 0.014	1.594 ± 0.023	1.036 ± 0.055	0.036 ± 0.055	2861 ± 572	
NGC 6268	8.343 ± 0.052	1.409 ± 0.023	1.562 ± 0.050	0.044 ± 0.045	536 ± 107	
NGC 637	7.265 ± 0.054	2.316 ± 0.088	1.962 ± 0.027	0.003 ± 0.048	430 ± 86	
NGC 6425	8.712 ± 0.024	0.969 ± 0.011	1.094 ± 0.070	0.050 ± 0.059	415 ± 83	
NGC 6444	8.451 ± 0.383	1.638 ± 0.087	1.616 ± 0.148	0.188 ± 0.065	630 ± 126	
NGC 6475	8.667 ± 0.001	0.273 ± 0.001	0.204 ± 0.001	0.114 ± 0.001	791 ± 158	767 ± 153
NGC 6520	7.937 ± 0.304	1.572 ± 0.064	1.337 ± 0.066	0.162 ± 0.069	555 ± 111	
NGC 6568	8.891 ± 0.025	1.019 ± 0.008	0.828 ± 0.062	0.151 ± 0.041	784 ± 156	
NGC 659	7.374 ± 0.089	2.634 ± 0.058	2.174 ± 0.047	0.083 ± 0.055	1094 ± 218	
NGC 6604	6.809 ± 0.057	1.935 ± 0.037	2.881 ± 0.037	0.103 ± 0.077	871 ± 174	
NGC 6633	8.901 ± 0.175	0.391 ± 0.002	0.549 ± 0.238	0.117 ± 0.043	512 ± 102	
NGC 6694	8.001 ± 0.159	1.675 ± 0.037	1.892 ± 0.029	0.173 ± 0.024	1208 ± 241	
NGC 6709	8.197 ± 0.049	1.043 ± 0.006	1.082 ± 0.023	0.047 ± 0.021	679 ± 135	687 ± 137
NGC 6728	8.762 ± 0.041	1.699 ± 0.021	0.876 ± 0.092	0.122 ± 0.049	1170 ± 234	1201 ± 240
NGC 6793	8.517 ± 0.169	0.583 ± 0.002	1.170 ± 0.057	0.126 ± 0.053	409 ± 81	
NGC 6811	9.003 ± 0.012	1.107 ± 0.007	0.255 ± 0.042	0.021 ± 0.025	646 ± 129	646 ± 129
NGC 6830	7.722 ± 0.212	2.024 ± 0.046	1.857 ± 0.034	0.159 ± 0.018	699 ± 139	
NGC 6866	8.892 ± 0.031	1.377 ± 0.021	0.514 ± 0.078	0.063 ± 0.064	449 ± 89	
NGC 6910	6.989 ± 0.040	1.640 ± 0.031	3.311 ± 0.101	0.030 ± 0.039	1528 ± 305	
NGC 6913	6.921 ± 0.037	1.636 ± 0.047	2.832 ± 0.163	0.003 ± 0.072	903 ± 180	
NGC 6939	9.183 ± 0.017	1.719 ± 0.040	1.397 ± 0.034	0.007 ± 0.036	2031 ± 406	
NGC 6940	9.022 ± 0.017	1.000 ± 0.009	0.709 ± 0.055	0.008 ± 0.045	1393 ± 278	1645 ± 329
NGC 6991	9.157 ± 0.013	0.551 ± 0.010	0.320 ± 0.052	0.070 ± 0.032	672 ± 134	610 ± 122
NGC 6997	8.631 ± 0.081	0.857 ± 0.013	2.038 ± 0.092	0.124 ± 0.088	535 ± 107	
NGC 7039	7.124 ± 0.037	0.739 ± 0.006	0.517 ± 0.079	0.031 ± 0.051	218 ± 43	
NGC 7062	8.650 ± 0.166	2.124 ± 0.059	1.679 ± 0.076	0.036 ± 0.041	568 ± 113	
NGC 7063	8.187 ± 0.169	0.656 ± 0.003	0.325 ± 0.039	0.002 ± 0.025	131 ± 26	
NGC 7067	7.085 ± 0.044	4.654 ± 0.167	2.565 ± 0.034	0.083 ± 0.047	701 ± 140	
NGC 7082	8.225 ± 0.099	1.295 ± 0.016	0.985 ± 0.052	0.028 ± 0.065	847 ± 169	
NGC 7086	7.741 ± 0.230	1.555 ± 0.025	2.325 ± 0.045	0.005 ± 0.047	2152 ± 430	
NGC 7092	8.565 ± 0.142	0.327 ± 0.023	0.047 ± 0.004	0.179 ± 0.132	331 ± 66	
NGC 7128	7.189 ± 0.090	3.133 ± 0.184	2.941 ± 0.031	0.046 ± 0.031	1366 ± 273	
NGC 7142	9.502 ± 0.031	2.168 ± 0.069	1.429 ± 0.065	0.099 ± 0.067	3434 ± 686	
NGC 7160	7.260 ± 0.136	0.894 ± 0.015	1.188 ± 0.079	0.036 ± 0.055	205 ± 41	
NGC 7209	8.625 ± 0.095	1.178 ± 0.017	0.699 ± 0.089	0.048 ± 0.064	1087 ± 217	982 ± 196

Table A1 continued from previous page

Name	log(age)	Dist. (kpc)	Av. (mag.)	FeH	$M_{Tint}(m_{\odot})$	$M_{Tdet}(m_{\odot})$
NGC 7226	8.591 ± 0.311	4.098 ± 0.250	1.856 ± 0.151	0.126 ± 0.032	432 ± 86	
NGC 7235	7.148 ± 0.055	3.112 ± 0.104	2.702 ± 0.030	0.125 ± 0.038	1635 ± 327	
NGC 7243	8.130 ± 0.084	0.864 ± 0.005	0.803 ± 0.042	0.004 ± 0.037	587 ± 117	
NGC 7245	8.796 ± 0.043	2.798 ± 0.094	1.288 ± 0.074	0.085 ± 0.033	1186 ± 237	
NGC 7296	8.400 ± 0.176	2.410 ± 0.058	0.793 ± 0.076	0.089 ± 0.057	642 ± 128	
NGC 7423	9.124 ± 0.042	3.688 ± 0.125	2.111 ± 0.098	0.186 ± 0.059	776 ± 155	
NGC 743	7.823 ± 0.304	1.045 ± 0.025	1.768 ± 0.089	0.001 ± 0.055	178 ± 35	
NGC 744	8.343 ± 0.135	1.265 ± 0.026	1.268 ± 0.112	0.046 ± 0.041	315 ± 63	
NGC 7510	7.020 ± 0.031	2.950 ± 0.115	3.065 ± 0.038	0.187 ± 0.056	2997 ± 599	
NGC 7762	9.206 ± 0.024	0.931 ± 0.014	2.543 ± 0.040	0.052 ± 0.051	1394 ± 278	
NGC 7790	7.457 ± 0.295	2.853 ± 0.074	1.931 ± 0.033	0.109 ± 0.048	1273 ± 254	
NGC 886	8.510 ± 0.110	0.988 ± 0.013	1.825 ± 0.082	0.017 ± 0.077	613 ± 122	
NGC 957	7.375 ± 0.079	2.050 ± 0.070	2.291 ± 0.014	0.029 ± 0.052	2071 ± 414	
Patchick 3	9.141 ± 0.037	1.587 ± 0.049	1.365 ± 0.081	0.123 ± 0.074	213 ± 42	
Pismis 11	6.833 ± 0.101	2.211 ± 0.190	3.411 ± 0.085	0.006 ± 0.130	467 ± 93	
Pismis 12	9.072 ± 0.041	2.099 ± 0.090	2.022 ± 0.119	0.128 ± 0.081	911 ± 182	
Pismis 15	9.091 ± 0.049	2.089 ± 0.103	2.183 ± 0.048	0.042 ± 0.048	554 ± 110	
Pismis 27	6.948 ± 0.023	1.763 ± 0.067	2.161 ± 0.196	0.098 ± 0.057	205 ± 41	
Pismis 4	8.306 ± 0.058	0.677 ± 0.003	0.207 ± 0.028	0.051 ± 0.025	235 ± 47	
Pismis 5	7.002 ± 0.087	0.905 ± 0.011	1.586 ± 0.122	0.051 ± 0.058	332 ± 66	
Pismis 8	7.146 ± 0.131	1.747 ± 0.072	2.227 ± 0.059	0.037 ± 0.123	250 ± 50	
Pismis Moreno 1	7.046 ± 0.127	0.894 ± 0.016	1.898 ± 0.049	0.054 ± 0.091	164 ± 32	
Platais 8	7.709 ± 0.050	0.135 ± 0.001	0.055 ± 0.063	0.153 ± 0.037	129 ± 25	
Platais 9	7.836 ± 0.071	0.187 ± 0.002	0.253 ± 0.092	0.005 ± 0.042	136 ± 27	
Pozzo 1	7.105 ± 0.074	0.343 ± 0.008	0.269 ± 0.059	0.042 ± 0.044	610 ± 122	
RSG 1	8.383 ± 0.105	0.310 ± 0.014	0.736 ± 0.069	0.101 ± 0.068	179 ± 35	
RSG 5	7.758 ± 0.030	0.329 ± 0.010	0.069 ± 0.006	0.077 ± 0.054	259 ± 51	
Roslund 3	8.020 ± 0.075	1.617 ± 0.028	1.149 ± 0.059	0.112 ± 0.080	496 ± 99	
Roslund 5	8.333 ± 0.138	0.533 ± 0.001	0.353 ± 0.023	0.049 ± 0.015	346 ± 69	
Roslund 6	8.514 ± 0.102	0.347 ± 0.004	0.062 ± 0.006	0.070 ± 0.016	502 ± 100	
Roslund 7	8.034 ± 0.163	1.219 ± 0.020	1.127 ± 0.064	0.009 ± 0.070	617 ± 123	
Ruprecht 1	8.685 ± 0.077	1.459 ± 0.020	0.736 ± 0.078	0.065 ± 0.059	403 ± 80	
Ruprecht 105	8.179 ± 0.270	1.858 ± 0.075	1.959 ± 0.171	0.112 ± 0.095	540 ± 108	
Ruprecht 107	8.090 ± 0.223	3.260 ± 0.084	1.652 ± 0.090	0.131 ± 0.030	533 ± 106	
Ruprecht 108	8.242 ± 0.193	0.961 ± 0.013	0.804 ± 0.067	0.111 ± 0.056	83 ± 16	
Ruprecht 111	9.058 ± 0.043	1.388 ± 0.025	1.706 ± 0.115	0.035 ± 0.062	740 ± 148	
Ruprecht 119	7.997 ± 0.160	1.882 ± 0.040	1.972 ± 0.083	0.180 ± 0.050	874 ± 174	
Ruprecht 120	7.391 ± 0.385	1.755 ± 0.082	2.407 ± 0.081	0.177 ± 0.057	221 ± 44	
Ruprecht 127	7.125 ± 0.064	2.137 ± 0.084	2.989 ± 0.044	0.153 ± 0.040	913 ± 182	
Ruprecht 128	8.716 ± 0.422	1.702 ± 0.109	2.759 ± 0.149	0.134 ± 0.097	846 ± 169	
Ruprecht 145	8.985 ± 0.020	0.588 ± 0.001	0.691 ± 0.073	0.062 ± 0.039	496 ± 99	444 ± 88
Ruprecht 148	7.439 ± 0.266	3.009 ± 0.248	2.292 ± 0.071	0.140 ± 0.063	388 ± 77	
Ruprecht 16	8.370 ± 0.107	2.610 ± 0.095	1.027 ± 0.050	0.046 ± 0.043	369 ± 73	
Ruprecht 171	9.482 ± 0.017	1.468 ± 0.028	0.934 ± 0.035	0.070 ± 0.048	2687 ± 537	2573 ± 514
Ruprecht 18	8.160 ± 0.198	2.305 ± 0.070	2.127 ± 0.057	0.053 ± 0.052	1263 ± 252	
Ruprecht 19	7.931 ± 0.125	1.371 ± 0.023	0.344 ± 0.031	0.048 ± 0.031	217 ± 43	
Ruprecht 25	8.933 ± 0.066	5.623 ± 0.188	1.859 ± 0.099	0.366 ± 0.041	400 ± 80	
Ruprecht 28	9.413 ± 0.099	3.679 ± 0.240	0.901 ± 0.147	0.045 ± 0.052	707 ± 141	
Ruprecht 34	8.340 ± 0.131	2.489 ± 0.058	1.104 ± 0.057	0.095 ± 0.032	374 ± 74	
Ruprecht 35	7.400 ± 0.219	3.249 ± 0.231	1.953 ± 0.034	0.153 ± 0.051	450 ± 90	
Ruprecht 4	8.850 ± 0.042	3.584 ± 0.069	1.666 ± 0.063	0.175 ± 0.046	738 ± 147	
Ruprecht 41	8.398 ± 0.352	3.676 ± 0.158	1.298 ± 0.074	0.114 ± 0.042	798 ± 159	
Ruprecht 42	8.452 ± 0.182	5.205 ± 0.128	1.550 ± 0.078	0.236 ± 0.038	689 ± 137	
Ruprecht 44	7.217 ± 0.055	4.139 ± 0.234	1.972 ± 0.026	0.232 ± 0.042	1171 ± 234	
Ruprecht 48	7.970 ± 0.255	3.223 ± 0.072	1.493 ± 0.040	0.115 ± 0.046	515 ± 103	
Ruprecht 50	8.922 ± 0.052	1.978 ± 0.072	0.330 ± 0.037	0.035 ± 0.057	81 ± 16	
Ruprecht 54	8.153 ± 0.360	3.839 ± 0.129	1.488 ± 0.123	0.158 ± 0.038	781 ± 156	
Ruprecht 58	8.698 ± 0.088	2.834 ± 0.051	1.068 ± 0.065	0.124 ± 0.020	605 ± 121	
Ruprecht 60	8.914 ± 0.052	4.116 ± 0.487	1.601 ± 0.190	0.116 ± 0.054	729 ± 145	
Ruprecht 63	8.545 ± 0.222	3.521 ± 0.192	1.756 ± 0.168	0.125 ± 0.021	899 ± 179	

Table A1 continued from previous page

Name	log(age)	Dist. (kpc)	Av. (mag.)	FeH	$M_{Tint}(m_{\odot})$	$M_{Tdet}(m_{\odot})$
Ruprecht 66	9.031 ± 0.055	4.154 ± 0.218	1.956 ± 0.061	0.144 ± 0.052	1220 ± 244	
Ruprecht 67	8.155 ± 0.149	1.439 ± 0.031	1.716 ± 0.038	0.012 ± 0.038	306 ± 61	
Ruprecht 68	9.244 ± 0.032	2.710 ± 0.036	1.415 ± 0.056	0.102 ± 0.046	1117 ± 223	
Ruprecht 71	7.426 ± 0.028	1.795 ± 0.056	1.250 ± 0.074	0.095 ± 0.076	481 ± 96	
Ruprecht 76	7.950 ± 0.341	1.911 ± 0.034	1.655 ± 0.072	0.014 ± 0.044	160 ± 32	
Ruprecht 8	8.553 ± 0.051	2.027 ± 0.061	1.411 ± 0.027	0.002 ± 0.057	336 ± 67	
Ruprecht 82	8.640 ± 0.104	1.995 ± 0.077	1.195 ± 0.096	0.006 ± 0.036	483 ± 96	
Ruprecht 84	8.317 ± 0.199	1.788 ± 0.049	0.741 ± 0.101	0.007 ± 0.050	347 ± 69	
Ruprecht 91	8.052 ± 0.116	1.022 ± 0.004	0.316 ± 0.040	0.014 ± 0.033	477 ± 95	
Ruprecht 93	8.503 ± 0.126	2.015 ± 0.050	0.890 ± 0.087	0.019 ± 0.056	502 ± 100	
Ruprecht 98	8.711 ± 0.078	0.459 ± 0.016	0.770 ± 0.154	0.127 ± 0.082	259 ± 51	
SAI 24	7.092 ± 0.080	1.930 ± 0.076	2.033 ± 0.040	0.016 ± 0.075	1072 ± 214	
SAI 25	7.043 ± 0.066	2.122 ± 0.189	3.346 ± 0.239	0.086 ± 0.063	959 ± 191	
SAI 4	7.536 ± 0.165	2.553 ± 0.073	1.829 ± 0.055	0.115 ± 0.032	368 ± 73	
SAI 47	7.599 ± 0.398	4.072 ± 0.483	2.112 ± 0.311	0.296 ± 0.027	235 ± 47	
SAI 81	8.367 ± 0.390	3.534 ± 0.160	1.892 ± 0.103	0.086 ± 0.067	849 ± 169	
SAI 86	8.814 ± 0.070	3.294 ± 0.063	2.057 ± 0.104	0.130 ± 0.051	628 ± 125	
SAI 91	8.536 ± 0.285	3.235 ± 0.094	1.754 ± 0.092	0.071 ± 0.017	419 ± 83	
SAI 94	9.006 ± 0.087	3.933 ± 0.208	2.216 ± 0.096	0.148 ± 0.050	393 ± 78	
Skiff J0507+30.8	9.114 ± 0.037	4.779 ± 0.197	1.815 ± 0.071	0.353 ± 0.066	810 ± 162	
Skiff J0614+12.9	8.536 ± 0.310	2.916 ± 0.117	1.924 ± 0.095	0.151 ± 0.054	312 ± 62	
Skiff J0619+18.5	7.952 ± 0.095	1.477 ± 0.026	1.167 ± 0.064	0.126 ± 0.036	423 ± 84	
Stephenson 1	7.789 ± 0.096	0.351 ± 0.001	0.432 ± 0.098	0.182 ± 0.088	204 ± 40	
Stock 1	8.733 ± 0.046	0.386 ± 0.010	0.330 ± 0.035	0.059 ± 0.074	346 ± 69	313 ± 62
Stock 10	8.132 ± 0.122	0.351 ± 0.001	0.683 ± 0.129	0.120 ± 0.096	194 ± 38	
Stock 14	7.251 ± 0.033	2.237 ± 0.050	0.882 ± 0.020	0.152 ± 0.027	557 ± 111	
Stock 20	7.250 ± 0.052	2.410 ± 0.058	1.476 ± 0.024	0.033 ± 0.035	298 ± 59	
Stock 21	8.597 ± 0.140	1.831 ± 0.055	1.718 ± 0.072	0.055 ± 0.074	170 ± 34	
Stock 23	8.152 ± 0.206	0.596 ± 0.001	0.972 ± 0.063	0.053 ± 0.079	301 ± 60	
Stock 24	8.092 ± 0.302	2.499 ± 0.090	1.838 ± 0.083	0.067 ± 0.054	439 ± 87	
Stock 4	8.276 ± 0.178	1.280 ± 0.023	0.730 ± 0.131	0.230 ± 0.062	415 ± 83	
Stock 5	8.067 ± 0.148	0.920 ± 0.005	1.678 ± 0.057	0.122 ± 0.078	446 ± 89	
Stock 7	8.175 ± 0.176	0.659 ± 0.002	1.743 ± 0.065	0.067 ± 0.039	260 ± 52	
Teutsch 1	7.661 ± 0.418	3.530 ± 0.098	2.052 ± 0.115	0.253 ± 0.016	314 ± 62	
Teutsch 103	8.662 ± 0.103	2.438 ± 0.135	2.748 ± 0.068	0.027 ± 0.023	235 ± 47	
Teutsch 12	8.877 ± 0.054	3.516 ± 0.109	2.159 ± 0.083	0.204 ± 0.047	532 ± 106	
Teutsch 126	7.997 ± 0.076	1.921 ± 0.043	1.358 ± 0.047	0.051 ± 0.057	483 ± 96	
Teutsch 13	7.438 ± 0.111	3.722 ± 0.101	2.147 ± 0.040	0.297 ± 0.014	688 ± 137	
Teutsch 132	7.219 ± 0.068	3.122 ± 0.142	2.207 ± 0.059	0.212 ± 0.039	309 ± 61	
Teutsch 35	8.000 ± 0.001	0.491 ± 0.001	0.031 ± 0.001	0.010 ± 0.001	193 ± 38	203 ± 40
Teutsch 38	7.842 ± 0.100	0.639 ± 0.001	0.262 ± 0.059	0.004 ± 0.065	296 ± 59	
Teutsch 61	7.427 ± 0.247	2.454 ± 0.096	2.011 ± 0.052	0.113 ± 0.051	349 ± 69	
Tombaugh 1	9.121 ± 0.026	2.372 ± 0.048	0.869 ± 0.065	0.095 ± 0.057	810 ± 162	
Tombaugh 5	8.353 ± 0.097	1.545 ± 0.030	2.505 ± 0.027	0.020 ± 0.028	1544 ± 308	
Trumpler 1	7.420 ± 0.075	2.424 ± 0.049	1.815 ± 0.022	0.046 ± 0.050	557 ± 111	
Trumpler 12	8.891 ± 0.021	3.121 ± 0.125	0.782 ± 0.049	0.020 ± 0.055	711 ± 142	
Trumpler 14	6.720 ± 0.061	2.271 ± 0.099	1.786 ± 0.027	0.025 ± 0.056	1994 ± 398	
Trumpler 15	6.906 ± 0.051	2.296 ± 0.115	1.637 ± 0.059	0.013 ± 0.041	1052 ± 210	
Trumpler 19	9.590 ± 0.045	2.357 ± 0.049	0.629 ± 0.063	0.039 ± 0.035	2684 ± 536	
Trumpler 2	8.027 ± 0.155	0.669 ± 0.002	1.189 ± 0.044	0.042 ± 0.037	498 ± 99	
Trumpler 21	7.802 ± 0.120	1.264 ± 0.025	0.828 ± 0.036	0.073 ± 0.054	253 ± 50	
Trumpler 3	7.748 ± 0.113	0.659 ± 0.004	1.100 ± 0.052	0.025 ± 0.054	444 ± 88	
Trumpler 32	8.874 ± 0.036	1.605 ± 0.031	2.431 ± 0.020	0.079 ± 0.033	1422 ± 284	1480 ± 296
Trumpler 33	7.836 ± 0.154	1.333 ± 0.024	1.488 ± 0.081	0.061 ± 0.096	313 ± 62	
UBC 118	8.340 ± 0.111	1.435 ± 0.027	1.558 ± 0.059	0.091 ± 0.054	412 ± 82	
UBC 133	7.813 ± 0.174	1.450 ± 0.035	2.964 ± 0.034	0.187 ± 0.052	710 ± 142	
UBC 136	8.223 ± 0.161	1.348 ± 0.022	2.483 ± 0.095	0.180 ± 0.085	710 ± 142	
UBC 151	8.213 ± 0.207	1.628 ± 0.022	1.144 ± 0.064	0.129 ± 0.055	413 ± 82	
UBC 152	8.001 ± 0.225	1.281 ± 0.026	1.864 ± 0.092	0.155 ± 0.074	172 ± 34	
UBC 154	8.833 ± 0.076	2.936 ± 0.147	1.734 ± 0.091	0.005 ± 0.046	536 ± 107	

Table A1 continued from previous page

Name	log(age)	Dist. (kpc)	Av. (mag.)	FeH	$M_{Tint}(m_{\odot})$	$M_{Tdet}(m_{\odot})$
UBC 157	8.254 ± 0.086	1.149 ± 0.011	0.893 ± 0.028	0.001 ± 0.022	183 ± 36	
UBC 162	7.730 ± 0.385	2.044 ± 0.057	1.948 ± 0.058	0.005 ± 0.031	714 ± 142	
UBC 166	7.389 ± 0.120	2.960 ± 0.111	1.477 ± 0.039	0.037 ± 0.043	1287 ± 257	
UBC 169	8.475 ± 0.049	1.372 ± 0.030	0.591 ± 0.077	0.121 ± 0.045	136 ± 27	
UBC 172	8.350 ± 0.153	2.456 ± 0.032	1.231 ± 0.047	0.073 ± 0.037	982 ± 196	
UBC 175	8.655 ± 0.174	1.274 ± 0.019	1.076 ± 0.176	0.016 ± 0.112	299 ± 59	
UBC 177	8.101 ± 0.066	1.079 ± 0.027	2.221 ± 0.115	0.103 ± 0.081	191 ± 38	
UBC 178	6.920 ± 0.046	0.827 ± 0.005	2.114 ± 0.034	0.047 ± 0.070	576 ± 115	
UBC 179	8.325 ± 0.081	1.160 ± 0.010	1.935 ± 0.074	0.156 ± 0.071	426 ± 85	
UBC 194	8.486 ± 0.032	1.276 ± 0.028	0.772 ± 0.078	0.112 ± 0.063	308 ± 61	
UBC 198	7.475 ± 0.041	1.800 ± 0.034	1.485 ± 0.087	0.122 ± 0.048	883 ± 176	
UBC 237	8.498 ± 0.146	1.721 ± 0.044	1.200 ± 0.089	0.118 ± 0.063	511 ± 102	
UBC 245	7.274 ± 0.086	1.977 ± 0.074	1.644 ± 0.062	0.002 ± 0.033	561 ± 112	
UBC 249	8.178 ± 0.142	1.724 ± 0.036	1.004 ± 0.120	0.152 ± 0.044	715 ± 143	
UBC 251	7.881 ± 0.115	1.792 ± 0.020	1.550 ± 0.047	0.147 ± 0.062	478 ± 95	
UBC 253	8.332 ± 0.210	1.572 ± 0.017	1.048 ± 0.096	0.064 ± 0.046	306 ± 61	
UBC 270	7.908 ± 0.171	2.232 ± 0.080	1.213 ± 0.045	0.076 ± 0.039	758 ± 151	
UBC 290	8.019 ± 0.030	1.579 ± 0.025	0.992 ± 0.033	0.124 ± 0.069	1125 ± 225	
UBC 292	7.480 ± 0.057	2.053 ± 0.031	1.386 ± 0.029	0.130 ± 0.047	1044 ± 208	
UBC 300	8.540 ± 0.165	1.753 ± 0.050	2.168 ± 0.065	0.105 ± 0.051	500 ± 100	
UBC 303	8.829 ± 0.128	1.705 ± 0.059	1.711 ± 0.101	0.114 ± 0.042	419 ± 83	
UBC 31	7.321 ± 0.124	0.315 ± 0.012	0.846 ± 0.093	0.128 ± 0.062	358 ± 71	
UBC 316	8.684 ± 0.581	1.599 ± 0.037	2.714 ± 0.106	0.142 ± 0.057	267 ± 53	
UBC 319	8.069 ± 0.172	1.305 ± 0.020	1.799 ± 0.055	0.175 ± 0.074	609 ± 121	
UBC 340	7.413 ± 0.066	1.265 ± 0.024	2.376 ± 0.076	0.161 ± 0.050	436 ± 87	
UBC 347	8.727 ± 0.203	1.267 ± 0.034	3.004 ± 0.075	0.069 ± 0.078	232 ± 46	
UBC 356	8.174 ± 0.128	1.057 ± 0.009	1.743 ± 0.025	0.059 ± 0.066	202 ± 40	
UBC 36	8.679 ± 0.197	1.752 ± 0.075	1.345 ± 0.100	0.070 ± 0.043	107 ± 21	
UBC 361	7.858 ± 0.155	1.508 ± 0.021	2.144 ± 0.055	0.171 ± 0.071	410 ± 82	
UBC 364	8.719 ± 0.052	1.591 ± 0.067	1.925 ± 0.109	0.068 ± 0.048	258 ± 51	
UBC 366	8.651 ± 0.046	1.725 ± 0.059	0.975 ± 0.062	0.053 ± 0.045	164 ± 32	
UBC 373	7.216 ± 0.061	1.235 ± 0.014	3.124 ± 0.037	0.006 ± 0.053	201 ± 40	
UBC 378	8.714 ± 0.242	1.428 ± 0.045	2.106 ± 0.141	0.034 ± 0.058	375 ± 75	
UBC 381	8.003 ± 0.210	2.037 ± 0.049	1.902 ± 0.078	0.059 ± 0.067	190 ± 38	
UBC 382	8.340 ± 0.243	2.124 ± 0.051	1.226 ± 0.079	0.008 ± 0.036	325 ± 65	
UBC 386	6.894 ± 0.034	1.135 ± 0.025	1.505 ± 0.049	0.036 ± 0.029	219 ± 43	
UBC 387	8.569 ± 0.129	1.526 ± 0.026	1.746 ± 0.069	0.056 ± 0.079	166 ± 33	
UBC 389	8.068 ± 0.193	2.092 ± 0.040	1.641 ± 0.049	0.024 ± 0.047	231 ± 46	
UBC 395	7.487 ± 0.747	2.200 ± 0.311	2.117 ± 0.408	0.138 ± 0.030	631 ± 126	
UBC 396	7.132 ± 0.103	1.018 ± 0.010	2.679 ± 0.040	0.071 ± 0.049	128 ± 25	
UBC 397	7.064 ± 0.279	3.159 ± 0.257	2.693 ± 0.049	0.107 ± 0.062	735 ± 147	
UBC 41	7.984 ± 0.138	2.065 ± 0.098	1.489 ± 0.066	0.006 ± 0.076	140 ± 28	
UBC 413	7.883 ± 0.248	2.228 ± 0.093	2.051 ± 0.135	0.043 ± 0.065	213 ± 42	
UBC 422	7.397 ± 0.275	2.350 ± 0.135	2.272 ± 0.032	0.149 ± 0.030	1353 ± 270	
UBC 424	8.693 ± 0.205	1.957 ± 0.043	1.970 ± 0.074	0.139 ± 0.040	303 ± 60	
UBC 429	8.832 ± 0.309	2.412 ± 0.137	2.163 ± 0.132	0.197 ± 0.068	306 ± 61	
UBC 433	9.106 ± 0.018	4.048 ± 0.150	1.863 ± 0.079	0.306 ± 0.052	646 ± 129	
UBC 436	8.753 ± 0.092	2.886 ± 0.113	1.253 ± 0.106	0.179 ± 0.062	604 ± 120	
UBC 437	7.825 ± 0.313	1.756 ± 0.070	1.847 ± 0.087	0.122 ± 0.046	359 ± 71	
UBC 439	8.458 ± 0.042	2.572 ± 0.126	1.389 ± 0.029	0.175 ± 0.047	471 ± 94	
UBC 442	8.953 ± 0.074	3.864 ± 0.372	1.455 ± 0.152	0.202 ± 0.101	472 ± 94	
UBC 445	8.772 ± 0.100	2.450 ± 0.101	0.839 ± 0.155	0.182 ± 0.072	323 ± 64	
UBC 448	8.921 ± 0.109	2.925 ± 0.145	0.380 ± 0.071	0.189 ± 0.031	830 ± 166	
UBC 449	8.939 ± 0.086	3.505 ± 0.221	0.855 ± 0.107	0.152 ± 0.074	469 ± 93	
UBC 450	7.936 ± 0.158	2.647 ± 0.076	1.078 ± 0.025	0.130 ± 0.035	632 ± 126	
UBC 451	8.472 ± 0.057	1.707 ± 0.061	0.221 ± 0.043	0.100 ± 0.071	104 ± 20	
UBC 460	7.597 ± 0.071	2.610 ± 0.127	1.131 ± 0.050	0.111 ± 0.052	1038 ± 207	
UBC 462	8.290 ± 0.212	2.884 ± 0.132	0.578 ± 0.037	0.054 ± 0.069	601 ± 120	
UBC 467	9.143 ± 0.015	4.722 ± 0.135	0.527 ± 0.049	0.046 ± 0.071	353 ± 70	
UBC 472	9.049 ± 0.084	1.753 ± 0.052	2.209 ± 0.073	0.069 ± 0.135	189 ± 37	

Table A1 continued from previous page

Name	log(age)	Dist. (kpc)	Av. (mag.)	FeH	$M_{Tint}(m_{\odot})$	$M_{Tdet}(m_{\odot})$
UBC 475	8.109 ± 0.136	1.962 ± 0.042	0.820 ± 0.045	0.058 ± 0.071	241 ± 48	
UBC 479	7.248 ± 0.061	1.420 ± 0.032	1.338 ± 0.240	0.061 ± 0.082	364 ± 72	
UBC 483	7.501 ± 0.215	1.817 ± 0.037	2.033 ± 0.049	0.169 ± 0.085	235 ± 47	
UBC 484	8.127 ± 0.324	1.951 ± 0.065	1.575 ± 0.155	0.013 ± 0.059	235 ± 47	
UBC 485	8.646 ± 0.167	1.675 ± 0.035	1.546 ± 0.109	0.011 ± 0.073	242 ± 48	
UBC 493	8.913 ± 0.090	1.607 ± 0.062	1.071 ± 0.154	0.017 ± 0.091	154 ± 30	
UBC 496	8.195 ± 0.184	1.592 ± 0.032	0.566 ± 0.100	0.095 ± 0.046	102 ± 20	
UBC 499	7.369 ± 0.040	2.277 ± 0.050	1.314 ± 0.055	0.013 ± 0.042	773 ± 154	
UBC 500	8.309 ± 0.221	2.292 ± 0.051	1.318 ± 0.072	0.024 ± 0.042	589 ± 117	
UBC 502	8.678 ± 0.122	1.681 ± 0.057	0.748 ± 0.147	0.011 ± 0.074	330 ± 66	
UBC 503	9.100 ± 0.039	1.950 ± 0.053	0.798 ± 0.087	0.028 ± 0.053	121 ± 24	
UBC 514	9.495 ± 0.077	1.813 ± 0.038	0.552 ± 0.114	0.210 ± 0.064	268 ± 53	
UBC 520	8.750 ± 0.134	1.868 ± 0.046	1.567 ± 0.102	0.016 ± 0.067	251 ± 50	
UBC 521	8.753 ± 0.318	2.488 ± 0.260	2.338 ± 0.158	0.130 ± 0.090	512 ± 102	
UBC 527	8.308 ± 0.180	1.658 ± 0.017	1.077 ± 0.086	0.054 ± 0.067	168 ± 33	
UBC 532	7.807 ± 0.263	1.709 ± 0.088	2.667 ± 0.075	0.137 ± 0.077	319 ± 63	
UBC 533	8.378 ± 0.198	1.228 ± 0.021	0.882 ± 0.066	0.018 ± 0.042	81 ± 16	
UBC 534	8.049 ± 0.227	1.563 ± 0.040	1.587 ± 0.065	0.099 ± 0.066	294 ± 58	
UBC 557	7.584 ± 0.086	1.421 ± 0.034	1.629 ± 0.047	0.115 ± 0.044	352 ± 70	
UBC 563	8.161 ± 0.298	1.060 ± 0.013	1.896 ± 0.074	0.107 ± 0.082	129 ± 25	
UBC 57	9.217 ± 0.039	1.747 ± 0.068	1.541 ± 0.065	0.142 ± 0.064	192 ± 38	
UBC 574	8.615 ± 0.368	1.411 ± 0.052	2.699 ± 0.082	0.157 ± 0.046	1114 ± 222	
UBC 576	7.413 ± 0.404	1.285 ± 0.031	3.053 ± 0.169	0.018 ± 0.131	180 ± 36	
UBC 582	7.267 ± 0.053	1.098 ± 0.017	0.518 ± 0.050	0.044 ± 0.064	97 ± 19	
UBC 586	9.073 ± 0.103	2.540 ± 0.122	1.397 ± 0.115	0.008 ± 0.067	569 ± 113	
UBC 591	8.086 ± 0.233	2.067 ± 0.038	1.209 ± 0.072	0.025 ± 0.028	204 ± 40	
UBC 599	8.487 ± 0.206	4.079 ± 0.245	1.417 ± 0.064	0.269 ± 0.059	221 ± 44	
UBC 615	9.527 ± 0.087	2.624 ± 0.309	0.207 ± 0.014	0.184 ± 0.039	645 ± 129	
UBC 626	8.849 ± 0.058	4.370 ± 0.507	1.170 ± 0.208	0.167 ± 0.073	533 ± 106	
UBC 63	7.347 ± 0.030	1.478 ± 0.020	0.746 ± 0.045	0.106 ± 0.051	228 ± 45	
UBC 634	7.814 ± 0.243	2.645 ± 0.075	1.016 ± 0.061	0.117 ± 0.044	312 ± 62	
UBC 636	8.831 ± 0.070	2.699 ± 0.143	0.590 ± 0.068	0.058 ± 0.070	193 ± 38	
UBC 641	7.379 ± 0.176	3.210 ± 0.116	1.263 ± 0.083	0.124 ± 0.063	661 ± 132	
UBC 643	8.573 ± 0.299	3.396 ± 0.322	1.528 ± 0.344	0.055 ± 0.072	494 ± 98	
UBC 68	8.080 ± 0.133	1.920 ± 0.050	1.219 ± 0.049	0.131 ± 0.034	273 ± 54	
UBC 80	7.679 ± 0.145	2.047 ± 0.052	0.901 ± 0.048	0.085 ± 0.067	126 ± 25	
UFMG 34	8.937 ± 0.063	2.124 ± 0.141	3.219 ± 0.060	0.092 ± 0.076	798 ± 159	
UFMG 58	8.451 ± 0.087	5.046 ± 0.299	2.994 ± 0.033	0.111 ± 0.061	740 ± 148	
UFMG 59	7.899 ± 0.200	1.280 ± 0.022	1.207 ± 0.164	0.001 ± 0.102	70 ± 14	
UPK 12	8.393 ± 0.124	0.638 ± 0.001	0.362 ± 0.053	0.039 ± 0.039	109 ± 21	
UPK 155	8.196 ± 0.076	0.866 ± 0.006	1.248 ± 0.076	0.002 ± 0.056	260 ± 52	
UPK 16	8.345 ± 0.283	0.792 ± 0.006	0.482 ± 0.048	0.104 ± 0.083	129 ± 25	
UPK 169	7.173 ± 0.297	0.832 ± 0.017	2.442 ± 0.168	0.286 ± 0.166	358 ± 71	
UPK 17	8.674 ± 0.152	0.657 ± 0.001	1.718 ± 0.056	0.060 ± 0.068	294 ± 58	
UPK 178	8.179 ± 0.107	0.917 ± 0.014	2.268 ± 0.119	0.120 ± 0.090	132 ± 26	
UPK 18	8.788 ± 0.535	0.749 ± 0.003	1.034 ± 0.180	0.228 ± 0.026	102 ± 20	
UPK 180	8.245 ± 0.100	0.844 ± 0.009	1.257 ± 0.071	0.209 ± 0.060	181 ± 36	
UPK 21	8.880 ± 0.033	0.579 ± 0.001	1.448 ± 0.115	0.198 ± 0.131	195 ± 39	
UPK 219	8.305 ± 0.056	0.795 ± 0.006	1.519 ± 0.140	0.104 ± 0.182	96 ± 19	
UPK 220	7.477 ± 0.290	0.944 ± 0.009	2.784 ± 0.052	0.025 ± 0.097	922 ± 184	
UPK 23	8.066 ± 0.078	0.953 ± 0.012	1.501 ± 0.098	0.219 ± 0.155	146 ± 29	
UPK 230	7.800 ± 0.357	0.533 ± 0.003	1.407 ± 0.250	0.029 ± 0.120	88 ± 17	
UPK 24	8.736 ± 0.320	0.498 ± 0.001	1.349 ± 0.204	0.373 ± 0.166	105 ± 21	
UPK 265	8.322 ± 0.074	0.832 ± 0.006	2.100 ± 0.103	0.176 ± 0.062	235 ± 47	
UPK 28	7.461 ± 0.335	0.877 ± 0.021	3.255 ± 0.093	0.162 ± 0.062	270 ± 54	
UPK 282	8.406 ± 0.092	0.765 ± 0.003	0.312 ± 0.032	0.041 ± 0.027	63 ± 12	
UPK 29	8.546 ± 0.255	0.649 ± 0.005	2.682 ± 0.105	0.138 ± 0.093	168 ± 33	
UPK 294	8.305 ± 0.155	0.730 ± 0.003	2.090 ± 0.115	0.269 ± 0.066	183 ± 36	
UPK 296	8.428 ± 0.088	0.525 ± 0.004	0.355 ± 0.051	0.052 ± 0.085	124 ± 24	
UPK 312	8.713 ± 0.181	0.680 ± 0.009	1.284 ± 0.120	0.187 ± 0.080	87 ± 17	

Table A1 continued from previous page

Name	log(age)	Dist. (kpc)	Av. (mag.)	FeH	$M_{Tint}(m_{\odot})$	$M_{Tdet}(m_{\odot})$
UPK 33	8.028 ± 0.289	0.499 ± 0.006	2.186 ± 0.205	0.032 ± 0.089	106 ± 21	
UPK 333	8.835 ± 0.174	0.614 ± 0.025	1.277 ± 0.094	0.168 ± 0.039	175 ± 35	
UPK 379	8.143 ± 0.420	0.744 ± 0.004	0.788 ± 0.383	0.009 ± 0.168	176 ± 35	
UPK 38	7.023 ± 0.079	0.575 ± 0.002	2.319 ± 0.061	0.044 ± 0.065	75 ± 15	
UPK 381	8.604 ± 0.038	0.692 ± 0.004	0.314 ± 0.023	0.002 ± 0.041	143 ± 28	
UPK 385	7.436 ± 0.125	0.308 ± 0.002	0.677 ± 0.290	0.192 ± 0.145	61 ± 12	
UPK 394	8.492 ± 0.177	0.778 ± 0.005	0.337 ± 0.053	0.118 ± 0.032	126 ± 25	
UPK 40	8.678 ± 0.145	0.636 ± 0.065	1.132 ± 0.127	0.128 ± 0.054	197 ± 39	
UPK 418	8.000 ± 0.001	0.825 ± 0.001	0.062 ± 0.001	0.068 ± 0.001	131 ± 26	
UPK 42	8.428 ± 0.085	0.580 ± 0.001	1.710 ± 0.056	0.099 ± 0.029	229 ± 45	
UPK 429	8.000 ± 0.001	0.855 ± 0.001	0.010 ± 0.001	0.068 ± 0.001	362 ± 72	
UPK 431	8.000 ± 0.067	0.716 ± 0.002	0.093 ± 0.024	0.060 ± 0.044	258 ± 51	
UPK 433	8.584 ± 0.060	0.760 ± 0.005	0.376 ± 0.029	0.055 ± 0.042	209 ± 41	
UPK 436	7.724 ± 0.143	0.809 ± 0.001	0.465 ± 0.040	0.003 ± 0.039	328 ± 65	
UPK 445	7.163 ± 0.053	0.655 ± 0.003	0.727 ± 0.069	0.203 ± 0.067	189 ± 37	
UPK 45	8.280 ± 0.242	0.849 ± 0.009	1.057 ± 0.139	0.033 ± 0.103	167 ± 33	
UPK 46	8.465 ± 0.101	0.666 ± 0.002	0.789 ± 0.074	0.025 ± 0.097	144 ± 28	
UPK 467	8.000 ± 0.001	0.572 ± 0.001	0.010 ± 0.001	0.045 ± 0.001	227 ± 45	223 ± 44
UPK 495	8.987 ± 0.086	0.611 ± 0.018	0.257 ± 0.109	0.201 ± 0.039	244 ± 48	
UPK 50	8.215 ± 0.172	0.989 ± 0.012	1.498 ± 0.057	0.042 ± 0.017	321 ± 64	
UPK 502	8.458 ± 0.230	0.675 ± 0.002	0.184 ± 0.133	0.045 ± 0.035	102 ± 20	
UPK 508	8.535 ± 0.197	0.813 ± 0.004	0.922 ± 0.130	0.089 ± 0.075	116 ± 23	
UPK 524	8.642 ± 0.205	0.545 ± 0.028	0.285 ± 0.096	0.085 ± 0.061	273 ± 54	
UPK 528	8.454 ± 0.191	0.951 ± 0.006	0.945 ± 0.074	0.093 ± 0.054	169 ± 33	
UPK 533	8.454 ± 0.211	0.338 ± 0.009	0.086 ± 0.071	0.072 ± 0.070	112 ± 22	
UPK 535	7.723 ± 0.076	0.321 ± 0.011	0.250 ± 0.092	0.056 ± 0.057	209 ± 41	
UPK 537	8.347 ± 0.138	0.594 ± 0.001	0.703 ± 0.077	0.053 ± 0.081	243 ± 48	
UPK 54	8.305 ± 0.068	0.798 ± 0.007	1.252 ± 0.038	0.188 ± 0.084	326 ± 65	
UPK 542	8.773 ± 0.189	0.770 ± 0.106	0.638 ± 0.316	0.229 ± 0.030	99 ± 19	
UPK 55	8.488 ± 0.174	0.779 ± 0.004	0.761 ± 0.067	0.048 ± 0.058	192 ± 38	
UPK 552	8.437 ± 0.082	0.331 ± 0.008	0.095 ± 0.052	0.006 ± 0.027	95 ± 19	
UPK 560	8.726 ± 0.103	0.592 ± 0.026	0.200 ± 0.093	0.117 ± 0.046	360 ± 72	
UPK 562	8.367 ± 0.163	0.846 ± 0.088	0.309 ± 0.120	0.069 ± 0.083	330 ± 66	
UPK 567	8.659 ± 0.140	0.633 ± 0.002	0.690 ± 0.160	0.054 ± 0.074	149 ± 29	
UPK 578	8.906 ± 0.056	0.907 ± 0.012	0.881 ± 0.201	0.100 ± 0.125	155 ± 31	
UPK 585	8.451 ± 0.098	0.703 ± 0.001	0.446 ± 0.134	0.233 ± 0.093	113 ± 22	
UPK 604	7.022 ± 0.183	0.740 ± 0.011	1.364 ± 0.408	0.098 ± 0.160	95 ± 19	
UPK 605	8.575 ± 0.141	0.726 ± 0.005	0.203 ± 0.073	0.141 ± 0.054	127 ± 25	
UPK 613	8.387 ± 0.154	0.841 ± 0.019	0.656 ± 0.092	0.231 ± 0.122	117 ± 23	
UPK 614	8.473 ± 0.161	0.885 ± 0.004	0.491 ± 0.106	0.011 ± 0.038	148 ± 29	
UPK 617	8.292 ± 0.222	0.713 ± 0.002	0.601 ± 0.049	0.022 ± 0.028	118 ± 23	
UPK 62	8.360 ± 0.334	0.874 ± 0.013	3.753 ± 0.088	0.041 ± 0.073	213 ± 42	
UPK 621	8.174 ± 0.189	0.874 ± 0.002	1.101 ± 0.062	0.019 ± 0.045	488 ± 97	
UPK 626	8.529 ± 0.064	0.496 ± 0.001	0.753 ± 0.050	0.007 ± 0.036	124 ± 24	
UPK 629	8.054 ± 0.082	1.820 ± 0.178	1.688 ± 0.182	0.031 ± 0.044	489 ± 97	
UPK 640	7.386 ± 0.039	0.175 ± 0.001	0.321 ± 0.064	0.145 ± 0.046	385 ± 77	
UPK 65	8.396 ± 0.107	0.748 ± 0.001	1.406 ± 0.064	0.271 ± 0.102	111 ± 22	
UPK 654	8.517 ± 0.168	0.497 ± 0.001	0.458 ± 0.137	0.048 ± 0.058	105 ± 21	
UPK 82	8.119 ± 0.133	0.504 ± 0.018	0.379 ± 0.040	0.051 ± 0.065	212 ± 42	
UPK 84	9.056 ± 0.040	0.896 ± 0.006	0.231 ± 0.035	0.011 ± 0.044	242 ± 48	
UPK 93	8.766 ± 0.092	0.637 ± 0.040	0.410 ± 0.097	0.228 ± 0.043	166 ± 33	
UPK 94	8.626 ± 0.181	0.933 ± 0.012	1.211 ± 0.077	0.040 ± 0.071	147 ± 29	
vdBergh 130	6.742 ± 0.129	1.559 ± 0.123	2.450 ± 0.030	0.051 ± 0.157	391 ± 78	
vdBergh 80	6.933 ± 0.120	0.937 ± 0.018	2.108 ± 0.202	0.053 ± 0.080	249 ± 49	
vdBergh 92	6.830 ± 0.094	1.084 ± 0.014	0.972 ± 0.053	0.076 ± 0.032	827 ± 165	

This paper has been typeset from a \LaTeX file prepared by the author.